Intraseasonal variability of Indian Ocean sea surface temperature during boreal winter: Madden-Julian Oscillation versus submonthly forcing and processes

Weiqing Han,[1] Dongliang Yuan,[2] W. Timothy Liu,[3] and D. J. Halkides[1]

Received 30 June 2006; revised 20 October 2006; accepted 13 November 2006; published 3 April 2007.

[1] Intraseasonal variability of Indian Ocean sea surface temperature (SST) during boreal winter is investigated by analyzing available data and a suite of solutions to an ocean general circulation model for 1998–2004. This period covers the QuikSCAT and Tropical Rainfall Measuring Mission (TRMM) observations. Impacts of the 30–90 day and 10–30 day atmospheric intraseasonal oscillations (ISOs) are examined separately, with the former dominated by the Madden-Julian Oscillation (MJO) and the latter dominated by convectively coupled Rossby and Kelvin waves. The maximum variation of intraseasonal SST occurs at 10°S–2°S in the wintertime Intertropical Convergence Zone (ITCZ), where the mixed layer is thin and intraseasonal wind speed reaches its maximum. The observed maximum warming (cooling) averaged over (60°E–85°E, 10°S–3°S) is 1.13°C (−0.97°C) for the period of interest, with a standard deviation of 0.39°C in winter. This SST change is forced predominantly by the MJO. While the MJO causes a basin-wide cooling (warming) in the ITCZ region, submonthly ISOs cause a more complex SST structure that propagates southwestward in the western-central basin and southeastward in the eastern ocean. On both the MJO and submonthly timescales, winds are the deterministic factor for the SST variability. Short-wave radiation generally plays a secondary role, and effects of precipitation are negligible. The dominant role of winds results roughly equally from wind speed and stress forcing. Wind speed affects SST by altering turbulent heat fluxes and entrainment cooling. Wind stress affects SST via several local and remote oceanic processes.

Citation: Han, W., D. Yuan, W. T. Liu, and D. J. Halkides (2007), Intraseasonal variability of Indian Ocean sea surface temperature during boreal winter: Madden-Julian Oscillation versus submonthly forcing and processes, *J. Geophys. Res.*, *112*, C04001, doi:10.1029/2006JC003791.

1. Introduction

1.1. Atmospheric Intraseasonal Oscillations

[2] Atmospheric intraseasonal oscillations (ISOs; 10–90 day periods) in the tropical troposphere have been extensively studied in the past few decades. On 30–90 day timescales, ISOs are dominated by the Madden-Julian Oscillation (MJO) [*Madden and Julian*, 1971, 1972], which has global zonal wave numbers 1–3, propagates eastward over the Indian Ocean during boreal winter (November–April), and both eastward and poleward during boreal summer (May–October) [e.g., *Lau and Chan*, 1985; *Knutson and Weickmann*, 1987; *Wang and Rui*, 1990; *Hendon and Salby*, 1994; *Li and Wang*, 1994; *Wang and Xie*, 1997; *Webster et al.*, 2002]. On submonthly timescales, ISOs are dominated by convectively coupled westward propagating Rossby waves and eastward propagating Kelvin waves [*Wheeler and Kiladis*, 1999; *Chatterjee and Goswami*, 2004, and references therein], which has global zonal wave numbers 5–6 [*Kiladis and Weickmann*, 1997]. Their important component, the quasi-biweekly oscillation, propagates westward [*Murakami and Frydrych*, 1974; *Chen and Chen*, 1993; *Numaguti*, 1995], and it is suggested to be a convectively coupled, first meridional mode Rossby wave that is displaced by the mean flow southward (northward) by about 5° during winter (summer) [*Chatterjee and Goswami*, 2004].

[3] Interestingly, observations from the Bay of Bengal Monsoon Experiment (BOBMEX) showed that convection and winds on submonthly timescales are stronger than those on 30–90 day timescales during the Asian summer monsoon [*Bhat et al.*, 2001]. This led Bhat et al. to speculate that submonthly ISOs may be more important than the MJO in causing sea surface temperature (SST) variability in the Bay. During winter, submonthly winds are also stronger, although convection on both submonthly and MJO scales

[1]Department of Atmospheric and Oceanic Sciences, University of Colorado, Boulder, Colorado, USA.
[2]Institute of Oceanology, Chinese Academy of Sciences, Qingdao, China.
[3]Jet Propulsion Laboratory, California Institute of Technology, Pasadena, California, USA.

0148-0227/07/2006JC003791$09.00

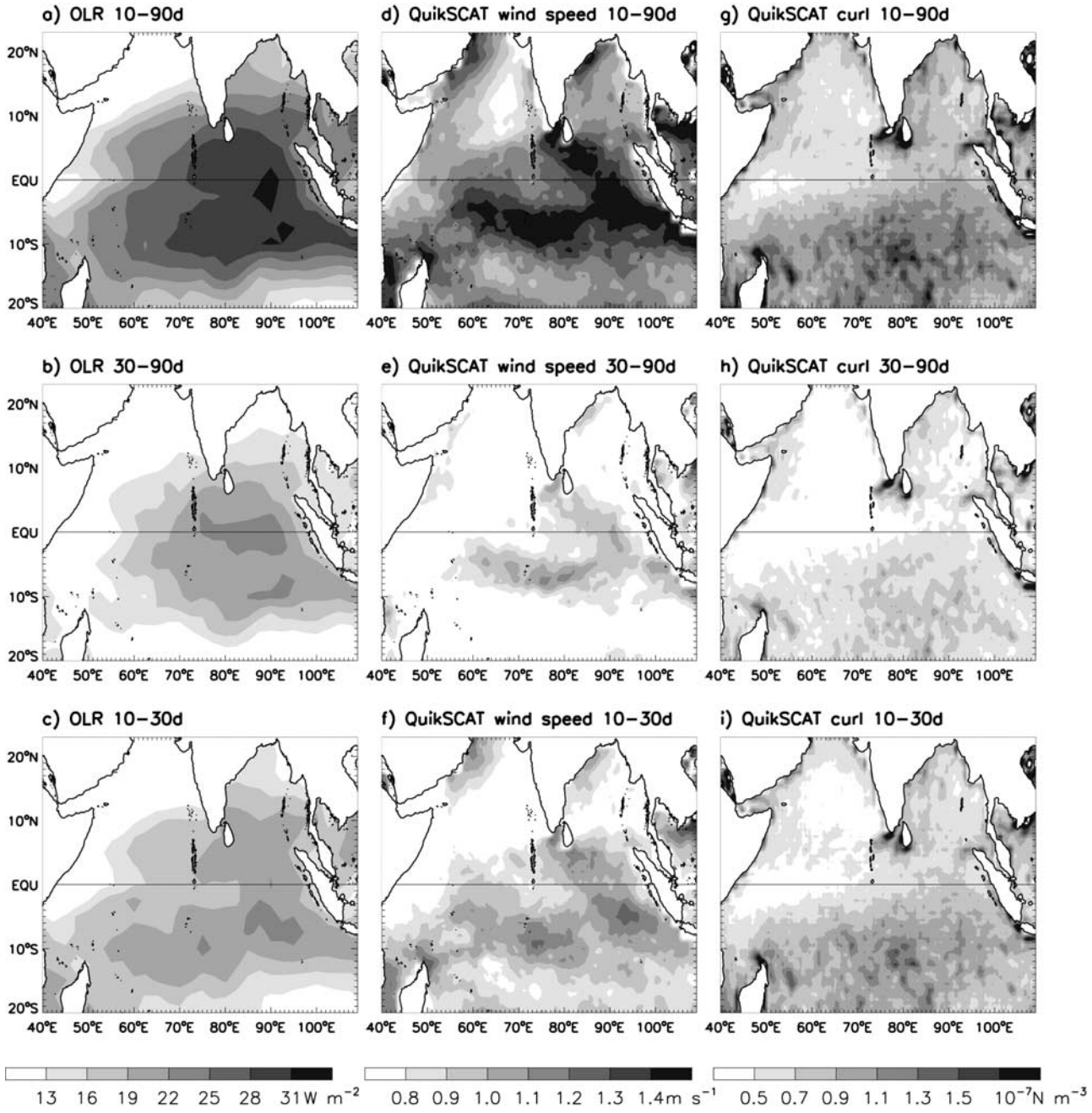

Figure 1. (a) Standard deviation (STD) of 10–90 day band-pass-filtered OLR over the tropical Indian Ocean during boreal winter (November–April) for the period 1999–2003 (see section 3.1 for a detailed description). (b) Same as Figure 1a except for 30–90 day OLR. (c) Same as Figure 1a but for 10–30 day OLR. (d) STD of 10–90 day band-passed QuikSCAT wind speed for the period 1999–2003. ERA40 winds are used before July 1999. (e) Same as Figure 1d but for 30–90 day wind speed. (f) Same as Figure 1d but for 10–30 day wind speed. (g) STD of 10–90 day band-passed QuikSCAT wind stress curl during 1999–2003. (h) Same as Figure 1g but for 30–90 day wind stress curl. (i) Same as Figure 1g except for 10–30 day wind stress curl. Units are W m^{-2} for OLR, m s^{-1} for wind speed, and 1×10^{-7} N m^{-3} for wind stress curl.

has similar strength (Figure 1) [see also *Vincent et al.*, 1998].

[4] The submonthly ISOs are known to have a large influence on the sudden onset, wet and dry phases of the Australian-Indonesian monsoon during boreal winter [*McBride*, 1987; *Wheeler and McBride*, 2005], and the Asian summer monsoon during boreal summer [e.g., *Sikka and Gadgil*, 1980; *Yasunari*, 1981; *Krishnamurti and Subramanyam*, 1982; *Webster*, 1983; *Wang and Xie*, 1997; *Lawrence and Webster*, 2002; *Webster and Hoyos*, 2004].

Combined with the MJO, they determine the amplitude and phase of the wet and dry spells [e.g., *Webster and Hoyos*, 2004; *Lau and Waliser*, 2005]. Recent studies have also shown that ISOs can affect the onset and termination of the Indian Ocean dipole [*Rao and Yamagata*, 2004; *Han et al.*, 2006a]. In dipole years [*Saji et al.*, 1999; *Webster et al.*, 1999; *Murtugudde et al.*, 2000], ISOs shift to the western Indian Ocean basin [*Gadgil et al.*, 2004; *Shinoda and Han*, 2005] and thus can affect the African rainfall. Moreover, many ISOs originating in the Indian Ocean can propagate eastward into the Pacific to impact ENSO [*Moore and Kleeman*, 1999; *McPhaden*, 1999; *Takayabu et al.*, 1999; *Kessler and Kleeman*, 2000; *Kiladis and Straub*, 2001].

[5] In recent years, the interaction of the ISOs and the ocean has been receiving increasing attention both for climate model simulation and prediction. Modeling studies demonstrate that air-sea coupling on intraseasonal timescales can improve ISO phase and propagation [*Flatau et al.*, 1997; *Wang and Xie*, 1998; *Woolnough et al.*, 2001; *Waliser et al.*, 1999; *Kemball-Cook and Wang*, 2001; *Inness and Slingo*, 2003; *Fu et al.*, 2003; *Sperber et al.*, 2005]. This improvement is important for monsoon and ENSO prediction (see above). Realistic simulation of the ISOs, however, is still a challenge for climate models [e.g., *Slingo et al.*, 1996; *Sperber et al.*, 2005; *Lin et al.*, 2006], which underlines our need for further understanding the coupled processes. Since the tropical ocean affects the atmosphere via SST, investigating intraseasonal SST variability induced by the ISOs is key to understand the coupled processes on intraseasonal timescales.

1.2. Indian Ocean Intraseasonal SST Variability

[6] Extensive observational and modeling studies on the Indian Ocean intraseasonal variability exist (see *Kessler* [2005] for a review). On the basis of earlier observations, *McPhaden* [1982] and *Krishnamurti et al.* [1988] suggested that winds associated with the MJO are the major cause for the 30–60 day variations of upper ocean temperature and SST; effects of heat fluxes induced by variability of air temperature and specific humidity are negligible [*Krishnamurti et al.*, 1988]. Field experiments from BOBMEX and JASMINE showed large-amplitude coherent evolutions of ISOs and SST in the Bay of Bengal [*Bhat et al.*, 2001; *Webster et al.*, 2002].

[7] Recent satellite observations provide a basin-wide view of intraseasonal SST variability. *Sengupta et al.* [2001a] analyzed satellite SST from the Tropical Rainfall Measuring Mission (TRMM) Microwave Imager [*Wentz et al.*, 2000], winds and satellite outgoing long-wave radiation (OLR), and found coherent development of SST, surface heat flux and convection associated with the Asian summer monsoon ISOs. *Harrison and Vecchi* [2001] analyzed TRMM SST and showed strong intraseasonal cooling over a large region of the south equatorial Indian Ocean during boreal winter of 1999. The amplitude of SST change was up to 3°C over a large area from peak cooling to peak warming of the event. They suggested that both air-sea heat flux and oceanic processes are important for the SST change. *Saji et al.* [2006] analyzed the intraseasonal cooling of the south equatorial region on the basis of 8 years (1998–2005) satellite data, and suggested that reduced solar radiation, enhanced evaporation and possibly strong entrainment all play a role, and local Ekman pumping may not be important. The maximum amplitude of SST composite based on strong cooling events is ~0.8°C.

[8] Empirical studies on the effects of the MJO have also been conducted using OLR and gridded reanalysis data sets [*Hendon and Glick*, 1997; *Jones et al.*, 1998; *Shinoda et al.*, 1998; *Woolnough et al.*, 2000]. These studies suggested that anomalous latent heat flux and surface insolation drive intraseasonal SST variations. The SST composites associated with strong MJO events have an amplitude of ~0.15°C [*Jones et al.*, 1998; *Shinoda et al.*, 1998], which is much weaker than that of recent studies.

[9] In the past few years, a large number of modeling studies have significantly advanced our understanding of the physical processes that account for intraseasonal SST variability. *Shinoda and Hendon* [1998] performed a one-dimensional, mixed layer model experiment by forcing the model with 10 individual MJO events along 5°S between 75°E and 175°E, a region where the MJO-induced SST variation attains maximum amplitude. They argued that latent heat seems less important than solar insolation in causing intraseasonal SST variability in the Indian Ocean basin, and effects of precipitation are trivial. Using an ocean general circulation model (OGCM), *Schiller and Godfrey* [2003] provided a detailed examination on how the Indian Ocean mixed layer and barrier layer [*Lukas and Lindstrom*, 1991; *Sprintal and Tomczak*, 1992] respond to atmospheric ISOs and how important these responses are in causing intraseasonal SST. Their analysis was based on ISO composites during the summer monsoon and showed a SST amplitude of ~0.2°C. *Waliser et al.* [2003, 2004] examined the impact of the composite canonical MJOs during both winter and summer, by performing a suite of OGCM experiments that were designed to isolate the effects of different forcings. They concluded that heat fluxes induced by the MJO, anomalous advection and mixed layer depth all contribute to the intraseasonal SST variability, whereas intraseasonal precipitation has a small influence. The amplitudes of intraseasonal SST forced by the canonical MJOs are smaller than 0.4°C.

[10] In contrast to the composite forcings, *Duvel et al.* [2004] performed an OGCM experiment and diagnosed the processes that determine the large-amplitude cooling associated with two individual ISO events during northern winter: January and March 1999. They concluded that the thin surface mixed layer near 5°S–10°S is enhanced in 1999 because of enhanced precipitation and anomalous wind stress curl, producing the maximum cooling there. For this region, intraseasonal SST variability is mainly driven by intraseasonal surface fluxes rather than by advection or exchanges with the subsurface.

[11] The above modeling studies either focused only on the MJO [e.g., *Shinoda et al.*, 1998; *Waliser et al.*, 2003, 2004] or examined the ISOs in general [*Schiller and Godfrey*, 2003; *Duvel et al.*, 2004]. Effects of submonthly ISOs on SST are much less studied. *Han et al.* [2006b] analyzed the TRMM SST and performed a series of OGCM experiments to isolate the effects of submonthly ISOs on Indian Ocean SST. They suggested that SST caused by submonthly ISOs can be as large as 0.5°C for strong events, and that winds are the primary force for the SST variability.

[12] Although extensive literatures exist, major processes that determine the strong intraseasonal cooling events are not conclusive and differ among different studies. This divergence of views suggests our need for a deeper and more complete understanding of the processes that control intraseasonal SST variability. Moreover, the relative importance of submonthly ISOs and the MJO in causing Indian Ocean SST variability is not yet known. Given that the wave number, structure, and propagation of the submonthly ISOs and the MJO are strikingly different, SST patterns induced by these variabilities are expected to be different. This difference in SST structures may, in turn, affect the phase and propagation of the submonthly ISOs and of the MJO in different ways, both having significant impacts on the monsoon. Indeed, understanding the impact of submonthly ISOs on SST is still in its initial stage, although submonthly ISOs are demonstrated to be the cause of the strong quasi-biweekly meridional currents in the equatorial Indian Ocean [*Reppin et al.*, 1999; *Sengupta et al.*, 2001b; *Masumoto et al.*, 2005; *Miyama et al.*, 2006].

1.3. Present Research

[13] The goals of this paper are to quantify the relative importance of intraseasonal winds, short-wave radiation and precipitation in driving intraseasonal SST variability over the tropical Indian Ocean during boreal winter, and examine the processes involved. Specifically, the effects of oceanic processes versus surface fluxes are estimated, and the impacts of the MJO and submonthly ISOs are separately discussed. In addition, detailed analysis of processes for specific cooling events, including the ones discussed by *Harrison and Vecchi* [2001] and *Duvel et al.* [2004], is provided.

[14] To accomplish the goals, we perform a suite of OGCM experiments using the Hybrid Coordinate Ocean Model (HYCOM) [*Bleck*, 2002]. The model is forced by realistic forcing fields and various filtered versions of them, for the period of 1998–2004 (section 2). In this paper, we focus only on examining the effects of northern winter (November–April) ISOs. Influences of northern summer ISOs (May–October) will be studied in a separate paper.

2. Data and Model

2.1. Data

[15] The $0.25^\circ \times 0.25^\circ$ 3 day mean SST from TRMM, 3 day QuikSCAT winds [*Tang and Liu*, 1996], and daily satellite observed OLR for the period of January 1998 to August 2004 are analyzed. Since QuikSCAT winds begin in July 1999, 3 day ECMWF reanalysis (ERA-40) winds are used before this time. To remove missing values, the TRMM SST was first interpolated onto $2.5^\circ \times 2.5^\circ$ grids. The few missing values left were then filled by linear spatial and temporal interpolation.

2.2. HYCOM

[16] Since HYCOM is documented in detail elsewhere [*Bleck*, 2002], only aspects relevant to this paper are discussed here. HYCOM has a hybrid vertical coordinate that is isopycnal in the open, stratified ocean, terrain-following coordinates in shallow coastal regions, and z coordinates in the mixed layer and unstratified seas. The feasibility of the hybrid coordinate approach for handling both deep and shallow regions throughout the annual heating/cooling cycle has been demonstrated for a North Atlantic basin by *Halliwell* [1998, 2004].

[17] Our version of HYCOM is configured to the tropical Indian Ocean north of 30°S, with a horizontal resolution of $0.5^\circ \times 0.5^\circ$ and realistic bottom topography [*Han et al.*, 2004, 2006a, 2006b; *Han*, 2005]. Vertically, 18 sigma layers are chosen with a fine resolution in the upper ocean to resolve better the structures of the mixed layer and thermocline, For example, the mean interface depths during the period of interest for the upper 10 layers are 3, 20, 137, 149, 156, 163, 171, 182, 198, 222 m averaged over (60°E–85°E, 10°S–3°S). The nonlocal K profile parameterization (KPP) is used for the boundary layer mixing scheme [*Large et al.*, 1994, 1997]. The diapycnal mixing coefficient is set to $(1 \times 10^{-7}\ \mathrm{m^2\ s^{-2}})/N$, where N is the buoyancy frequency. Isopycnal diffusivity and viscosity values are formulated as $u_d\Delta_x$, where Δ_x is the local horizontal mesh size and u_d is $0.03\ \mathrm{m\ s^{-1}}$ for momentum and $0.015\ \mathrm{m\ s^{-1}}$ for temperature and salinity. In regions of large shear, isopycnal viscosity is set proportional to the product of mesh size squared and total deformation [*Bleck*, 2002]; the proportionality factor here is 0.6. Short-wave radiation penetration is included with Jerlov water type IA [*Jerlov*, 1976].

[18] No-slip conditions are applied along continental boundaries. Near the southern boundary, a sponge layer with a width of 5° (25°S–30°S) is applied that relaxes model temperature and salinity fields to *Levitus and Boyer* [1994] and *Levitus et al.* [1994] climatology. Lateral boundary forcing due to the Indonesian Throughflow and Bay of Bengal rivers is included by relaxing the model temperature and salinity to Levitus data in the corresponding regions, but there are no inflow and outflow across the boundaries. Bottom topographic data are from the ETOPO5 smoothed over a $4^\circ \times 4^\circ$ bin.

[19] Surface forcing fields used to force HYCOM are the 3 day QuikSCAT winds, net short-wave and long-wave radiative fluxes from the International Satellite Cloud Climatology Project flux data (ISCCP-FD) [*Zhang et al.*, 2004], Climate Prediction Center Merged Analysis of Precipitation (CMAP) pentad data [*Xie and Arkin*, 1996], and ERA-40 air temperature and specific humidity for the period of interest (1998–2004). There are a few exceptions to these fields. Because QuikSCAT winds begin in July 1999, ERA-40 winds are used before this time. The two wind fields match well because the ERA-40 winds assimilated satellite data including the QuikSCAT winds. Because the ISCCP fluxes are available only to August 2001, values after this time are estimated using the OLR data by regressing the OLR onto ISCCP fluxes. First, regression coefficients are estimated on the basis of daily OLR and ISCCP short-wave and long-wave fluxes during 1988–2001. These coefficients, together with the OLR during August 2001 to November 2004, are used to estimate the fluxes after August 2001. This procedure is essentially the same as *Shinoda et al.* [1998] and *Schiller and Godfrey* [2003], and the regressed fields are shown to be in excellent agreement with the observed ISCCP fluxes during 1988–2001 (not shown). Similarly, because the ERA-40 air temperature and specific humidity are available only to 2001, their values smoothly transit to the NCEP/NCAR

Table 1. Suite of HYCOM Experiments for the Period of 1998–2004[a]

Experiment	Forcing	Description
MR	3-day mean	complete
EXP1	low-passed 105-day	remove all ISOs
EXP2	low-passed 30-day	remove submonthly ISOs
EXP3	low-passed wind stress	remove ISO wind stress
EXP4	low-passed winds (stress plus speed)	remove ISO stress and speed
EXP5	low-passed short-wave flux	remove ISO short-wave flux
EXP6	low-passed precipitation	remove ISO precipitation

[a]See text for detailed description. Unless specified, otherwise ISOs are removed with the 105-day low-pass filter.

reanalysis fields afterward. Winds, air temperature and specific humidity, together with HYCOM SST are used to calculate surface latent and sensible heat fluxes.

[20] These choices are based on either the best available data sets for the period of interest or a comparison of products. The HYCOM SST forced by QuikSCAT winds agrees better with the TRMM data than the SST forced by NCEP winds in the interior Indian Ocean (not shown). A comparison of precipitation fields for 1998–2001 from the TRMM, CMAP, and the ERA-40 reanalysis shows that CMAP represents the TRMM precipitation pattern more faithfully than the ERA-40 product. The regressed ISCCP short-wave radiation and its intraseasonal variation compare reasonably well with the TRITON data at (90°E, 1.5°S). The correlation coefficient between the ISCCP net and TRITON downward short-wave flux is 0.75 for the period of October 2001 to June 2004. The standard deviation (STD) is 50 W m^{-2} for TRITON and 42 W m^{-2} for ISCCP during the same period of time. By assuming a mean oceanic reflection rate of 3%, the TRITON net short-wave flux is about 49 W m^{-2}. This suggests that ISCCP flux may underestimate the intraseasonal variations by ~14%. Suitability of these forcing fields is further demonstrated by the reasonable model/data agreements shown in sections 3.3 and 3.4.

2.3. Experiments

[21] The model is restarted from the already spun-up HYCOM solution that was forced by ERA-40 fields [*Han et al.*, 2006a] on 1 January 1998 for each of the solutions discussed below, and integrated forward until November 2004. See *Han et al.* [2006a] for a detailed description of the model spin up. Table 1 lists the suite of parallel experiments reported in this paper.

[22] The main run (MR) is forced by the 3 day mean fields, and is the most complete solution in the suite. To exclude atmospheric intraseasonal variability entirely, in Experiment 1 (EXP1) HYCOM is forced by low-passed fields using a Lanczos filter [*Duchon*, 1979] with a half-power period at 105 days. The choice of using 105 days instead of 90 days is because the ocean attains a large dynamical response near the 90 day period [*Han et al.*, 2001; *Schouten et al.*, 2002; *Han*, 2005]. The MJO, however, is not sensitive to these choices. *Hendon et al.* [1998] tested the half-power period at 90 days and 120 days, and obtained essentially the same MJO signals. *Saji et al.* [2006] tested a 20–200 day bandwidth to avoid the possibility of successive intraseasonal events being artificially smeared into each other [*Matthews*, 2000]. They noted, however, that the results do not change when they use 30–90 day band-pass filtering. Our analysis shows that all the cooling events identified by previous studies are clearly shown in our 10–90 day band-passed fields without smearing into each other (section 3).

[23] The filter employs 121 weights, giving very sharp cutoffs with negligible Gibbs oscillation (not shown) and thus effectively excludes the ISOs [see also *Kiladis and Weickmann*, 1997]. The difference solution, $MR - EXP1$, measures the impact of all ISOs. To exclude atmospheric submonthly variability only, EXP2 is performed. It is the same as EXP1 except that HYCOM is forced by the 30 day low-passed fields. The differences, $MR - EXP2$ and $EXP2 - EXP1$, estimate the impact of ISOs on submonthly and MJO timescales, respectively. Experiments EXP3, EXP4, EXP5 and EXP6 are like the MR except forced by the 105 day low-passed wind stress, winds (wind stress and speed), short-wave radiation, and precipitation, respectively. Difference solutions $MR - EXP3$, $MR - EXP4$, $EXP3 - EXP4$, $MR - EXP5$ and $MR - EXP6$ isolates the effects of wind stress, total winds (stress plus speed), wind speed, short-wave flux and precipitation on intraseasonal timescales. Specific physical processes that are isolated by each of the above solutions are discussed in detail in section 3.4.

3. Results

[24] In section 3.1, the MJO and submonthly ISOs are discussed. In section 3.2, HYCOM MR is compared with observations to verify the model performance. In section 3.3, impacts of the MJO and submonthly ISOs on intraseasonal SST are estimated. Finally, in section 3.4 the processes that determine intraseasonal SST variability are examined.

3.1. MJO and Submonthly ISOs

[25] The left column of Figure 1 shows the standard deviations (STD) of OLR, which is used as a measure of signal strength, during winter for the entire ISO band (Figure 1a), the MJO band (Figure 1b), and the submonthly ISOs (Figure 1c) for the period of 1999–2003. To obtain each field, we first performed 10–90 day, 30–90 day, and 10–30 day band-pass filtering using the satellite observed daily OLR for the period of 1998–2004. To exclude the end point effects of the filter, only 1999–2003 filtered data are used to calculate the STD. The middle and right columns of Figure 1 show the corresponding STDs of QuikSCAT wind speed and wind stress curl.

[26] Strong intraseasonal variations of convection (Figures 1a–1c) occur in the eastern equatorial warm pool where mean SST exceeds 29°C (Figure 2), and in southern

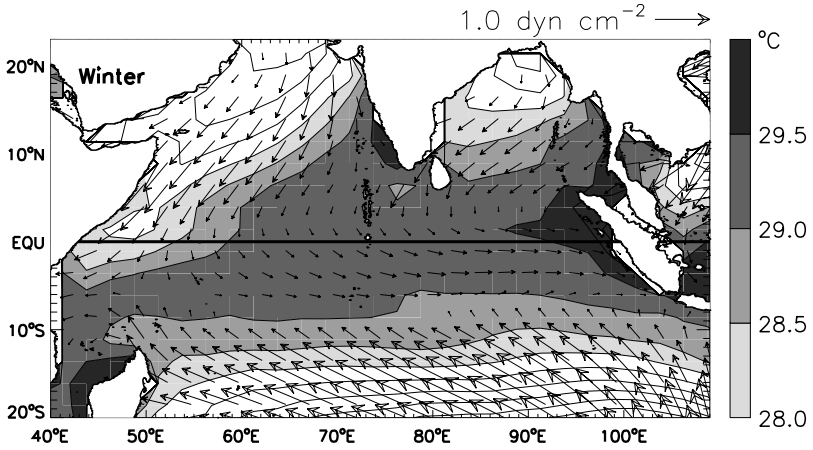

Figure 2. Wintertime (November–April) mean SST from TRMM (shading and line contours) and mean winds from QuikSCAT (arrows) for the period 1998–2003. ERA40 wind stress was used before July 1999. Units for SST are °C and for wind stress are dyn cm^{-2}.

tropical basin (12°S–2°S) where the intertropical convergence zone (ITCZ) is located. In these regions, intraseasonal wind speeds also attain maximum amplitudes (Figures 1d–1f). Intraseasonal wind stress curl also has large amplitudes over the ITCZ but reaches its maximum near 10°S–15°S (Figures 1g–1i). Wind speed and stress curl associated with the submonthly ISOs are stronger than those of the MJO.

3.2. Validation of the Simulated Intraseasonal SST

[27] Figures 3a and 3b plot the STDs of TRMM (left column) and HYCOM MR (right) intraseasonal SST calculated from the entire data record (both winter and summer) of 1999–2003. The most striking feature of Figure 3 is that the largest SST variations occur in a large region south of the equator, which coincide with the strong convection and winds associated with the ISOs in the wintertime ITCZ area (Figures 1 and 2) [*Saji et al.*, 2006]. The SST maxima result mainly from the wintertime SST variation (Figures 3c–3d), and maximum SST change shifts to the northern hemisphere during summer (not shown).

[28] Interestingly, although submonthly ISOs are associated with stronger winds than the MJO, SST variations at 30–90 day periods are generally larger than those at submonthly periods, especially in the region of the STD maxima (compare Figures 3e–3f with Figures 3g–3h). The maximum SST variations over the ITCZ, the frequency shift between the forcing and response, effects of the MJO and submonthly ISOs and associated processes are discussed in detail in section 3.4.

[29] Apparently, the basin-wide patterns of the observed SST variations are well captured by HYCOM MR, albeit with some quantitative differences. To further quantify the model/data comparison, we plotted the time series of 10–90 day SST (Figure 4) in three representative regions of the Indian Ocean (boxed regions in Figure 3c). In all three regions, intraseasonal SST variations are reasonably simulated (thick solid and dashed curves). The data/model correlation coefficients (r) are 0.82 near the ITCZ (region 1), 0.63 in the eastern Indian Ocean warm pool (region 2), and 0.68 for the western-central equatorial basin (region 3) above 95% significance. The two cold events during January–March 1999 over the ITCZ region, which were studied by *Harrison and Vecchi* [2001] and *Duvel et al.* [2004], are well simulated by the model. These cooling events occur every winter, and all events with amplitudes exceeding 1 STD are reasonably captured by HYCOM (Figure 4a). At 30–90 day MJO periods, the observed/modeled SST agrees even better (Figure 5a). At submonthly period, the SST variations are also reasonably simulated (Figure 5b). A further validation of the model for specific events is provided in section 3.4.

[30] The reasonable agreement between TRMM SST and HYCOM MR solution suggests that the model captures the major processes that determine the intraseasonal SST variability, and thus is suitable for the present study. There are, however, quantitative model/data differences. For example, amplitudes of SST STD from HYCOM are larger than those from TRMM in the ITCZ region (Figure 3). This is likely because HYCOM produces a thinner mixed layer than that calculated from WOA05 climatology and ARGO data in this area (Figure 6). Note that there are only 14 ARGO profiles in the area of interest during summer 2002. The larger ARGO/HYCOM difference this year may result partly from insufficient data sampling. Model/data discrepancies may also result from the difference between the TRMM skin temperature and model bulk layer temperature, the uncertainty in the model forcing fields, and data and model errors. In coastal regions, the modeled SST variations appear to be much weaker. This is possibly because of the artificial interpolation of QuikSCAT winds to land where their values are zero.

3.3. Impact of Atmospheric ISOs

[31] The intraseasonal SST from TRMM and HYCOM shown in Figures 3 and 4 includes the effects of both ISO forcing and internal variability due to instabilities [e.g., *Tsai et al.*, 1992; *Jochum and Murtugudde*, 2005]. To isolate the effects of ISOs, we first obtain the difference solution *MR* − *EXP*1 (section 2.3), and then apply the 10–90 day band-pass filter. The SST forced by the ISOs are shown as thin solid curves in Figure 4. Consistent with the work of *Waliser et al.* [2003], large-scale intraseasonal SST varia-

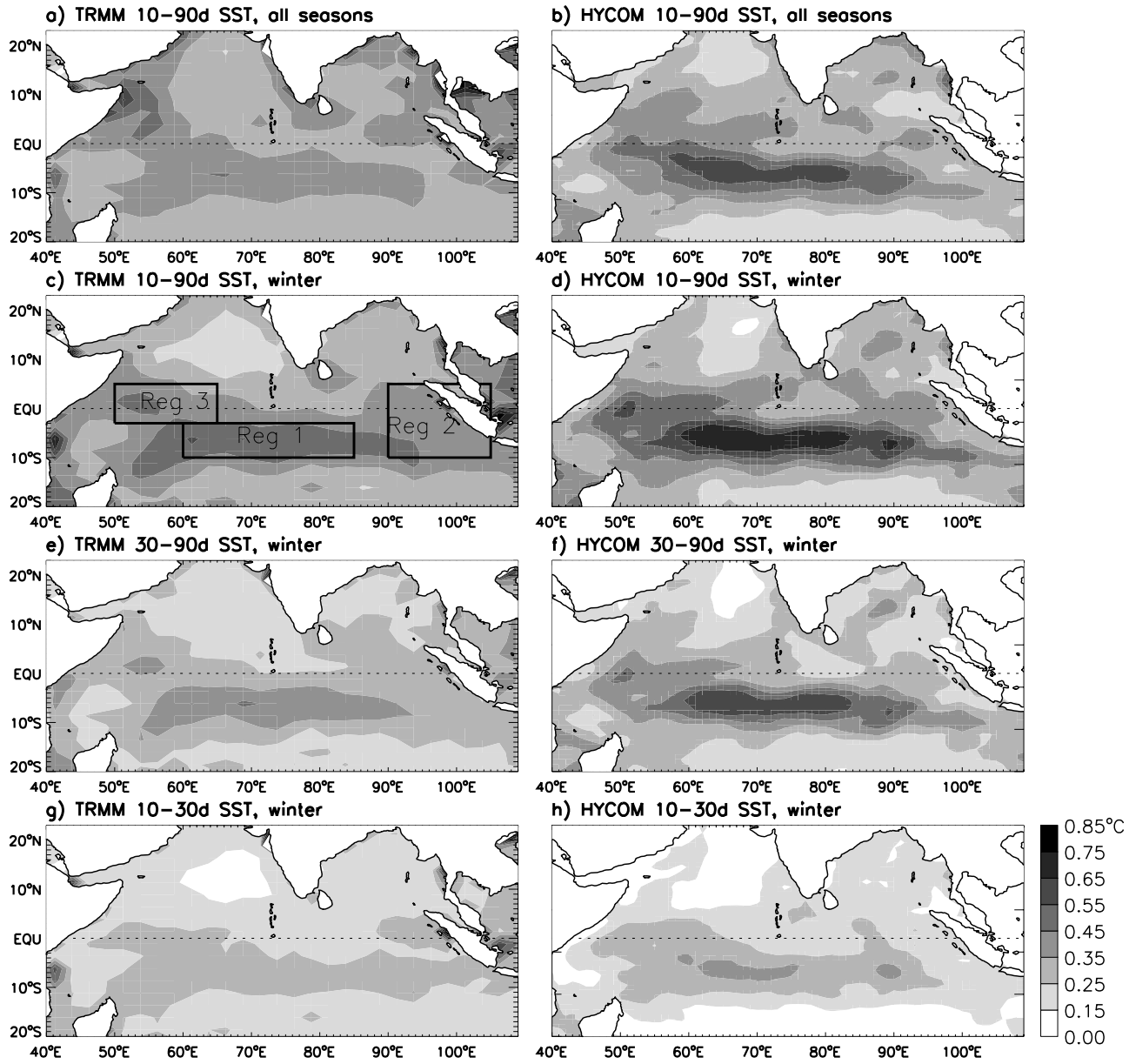

Figure 3. (a) STDs of 10–90 day TRMM SST based on the entire data record of 1999–2003. (b) Same as Figure 3a but for HYCOM MR. (c) STDs of 10–90 day TRMM SST based on the winter data of 1999–2003. The three boxed regions represent the ITCZ (region 1), warm pool (region 2), and western-central equatorial basin (region 3) and are discussed in the text. (d) Same as Figure 3c but for HYCOM MR. (e) Same as Figure 3c but for 30–90 day TRMM SST. (f) Same as Figure 3e but for HYCOM MR. (g) Same as Figure 3c but for 10–30 day TRMM SST. (h) Same as Figure 3g but for HYCOM MR. Units are °C.

tions forced by the ISOs agree very well with that of the MR in all three regions (thin solid and dashed), especially in the ITCZ and warm pool areas where the correlation coefficients (r_m) between the two curves are 0.97 and 0.96 above 95% significance (Figures 4a–4b). In the western-central equatorial basin where instabilities often occur [e.g., *Kindle and Thompson*, 1989], quantitative differences between the two curves are somewhat larger, indicating the effects of instabilities; but the two curves also agree well, with correlation of 0.92 above 95% significance. Near the Somali current region where instabilities are strong, however, there are significant differences between the two curves (not shown). The correlation between the MR and ISO-forced SST on 10–90 day timescales drops to 0.55 for an averaged region of (45°E–50°E, 0°N–10°N).

[32] Similarly, examination of difference solutions *MR* − *EXP*1, *EXP*2 − *EXP*1 and *MR* − *EXP*2 shows that SST variations on the MJO and submonthly timescales are mainly forced by the corresponding ISOs in the ocean interior (not shown). Near the Somali current region, instabilities have a large effect on the 30–90 day SST. In this region, the correlation between the MR and MJO-forced

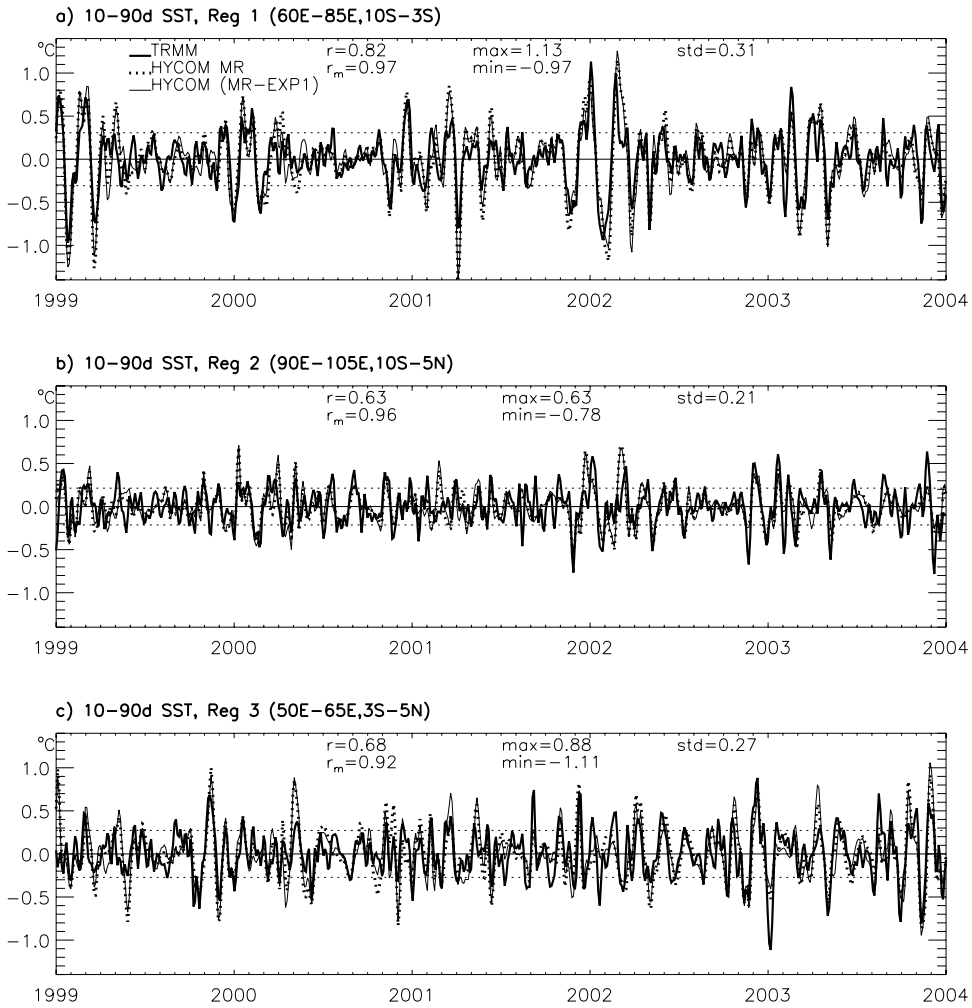

Figure 4. (a) Time series of 10–90 day SST averaged over (60°E–85°E, 10°S–3°S) in the ITCZ region (region 1 of Figure 3c) during 1999–2003. The thick solid and dashed curves show TRMM and HYCOM MR SST, respectively. The thin solid curve shows HYCOM SST forced by the ISOs. It is obtained by first taking the difference (*MR* − *EXP*1) and then applying the 10–90 day band-pass filter. (b) Same as Figure 4a but for the warm pool (90°E–105°E, 10°S–5°N), region 2 of Figure 3c. (c) Same as Figure 4a but for the western-central equatorial basin (50°E–65°E, 3°S–5°N), region 3 of Figure 3c. The two horizontal dashed curves in each plot show 1 STD of the TRMM SST. Units are °C.

SST is 0.41. On submonthly timescales, SST results mainly from ISO forcing even along the Somali current region, with a correlation of 0.91 between the MR and ISO forced SST averaged over (45°E–50°E, 0°N–10°N).

[33] These results demonstrate that intraseasonal SST variability over the tropical Indian Ocean interior results largely from ISO forcing, with internal variability playing a minor or negligible role [see also *Waliser et al.*, 2003]. Near Somali current region, however, effects of internal variability on 30–90 day SST are large and not negligible. Since our model has a 0.5° × 0.5° resolution, it can only resolve large-scale instabilities. A finer resolution is required for a more accurate examination of the internal variability.

[34] The ISO-induced SST variability attains its maxima in the ITCZ region (Figure 3), with an area-averaged warming (cooling) maximum of 1.13°C (−0.97°C) from TRMM during 1999–2003 (Figure 4a). These amplitudes are comparable with those of recent studies based on individual events [*Harrison and Vecchi*, 2001; *Duvel et al.*, 2004]. Composite SST based on strong cooling events shown in Figure 4a reaches the maximum amplitude of ∼0.8°C (not shown), which agrees with *Saji et al.* [2006] but is much stronger than the ∼0.15°C from earlier studies [e.g., *Jones et al.*, 1998; *Shinoda et al.*, 1998; *Schiller and Godfrey*, 2003]. This difference most likely results from the different composite technique used in the earlier studies, and the early versions of Reynolds data may also somewhat underestimate the SST amplitudes (T. Shinoda, personal communication, 2006). Earlier studies chose strong convection, rather than strong cooling events to perform the composites. This may significantly weaken the composite amplitude because different convective events can be associated with different spatial structures of SST. The STD from TRMM (HYCOM) for the ITCZ region for the 5 winters of 1999–2003 is 0.39°C (0.47°C) (Table 2).

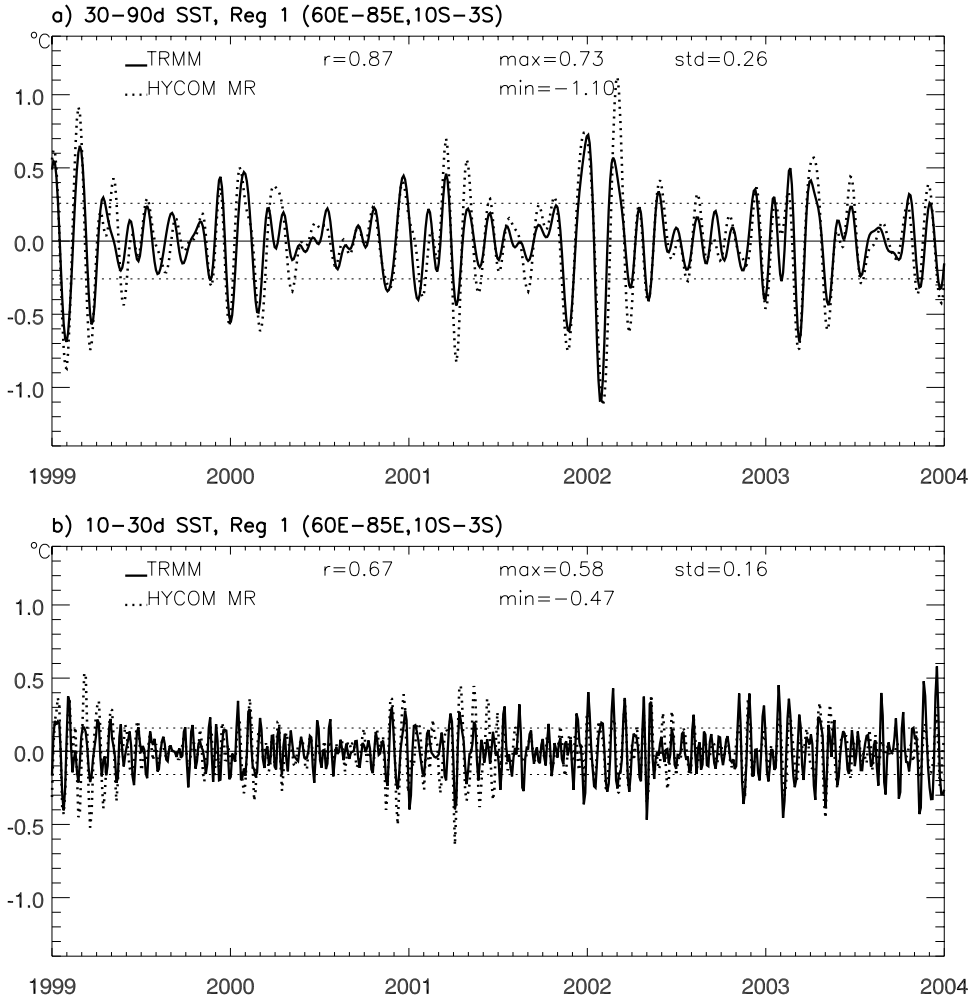

Figure 5. (a) Time series of TRMM (solid curve) and HYCOM (dashed curve) 30–90 day SST averaged over the ITCZ region (region 1) during 1999–2003. (b) Same as Figure 5a but for 10–30 day SST.

[35] In the western-central equatorial basin, intraseasonal SST variability is also large, with the maximum warming (cooling) of 0.88°C (−1.11°C) and wintertime STD of 0.30°C from TRMM and 0.32°C from HYCOM (Figure 4c and Table 2). In the warm pool region (Figure 4b), SST variations have smaller amplitudes, with warming (cooling) maxima of 0.63°C (−0.78°C) and STD of 0.25°C/0.23°C from TRMM/HYCOM. This amount of SST change, however, can be important in causing convection in the warm pool region where mean SST generally exceeds 29°–29.5°C (Figure 2).

[36] Likewise, on both the MJO and submonthly timescales, SST variations are strongest over the ITCZ, somewhat weaker in the western-central equatorial basin, and relatively weak in the warm pool region (Table 2). The differences among the three regions, however, are much smaller at the submonthly periods, with the wintertime TRMM STD of 0.19°C, 0.18°C, and 0.16°C in the ITCZ, western equatorial basin, and the warm pool (Table 2). While the MJO dominates the SST variability over the ITCZ region and thus is the major cause for the strong cooling events discussed by recent studies [*Harrison and Vecchi*, 2001; *Duvel et al.*, 2004; *Saji et al.*, 2006], in the warm pool and western-central equatorial basin SST variations caused by the MJO and submonthly ISOs are comparable.

3.4. Processes

3.4.1. General Analysis

[37] To quantify the relative importance of winds, wind stress, wind speed, solar radiation, and precipitation associated with the ISOs in forcing SST variability, Figures 7a and 7b show the 30–90 day, and Figures 7c and 7d show the 10–30 day SST variability due to each of the above forcings from the suite of HYCOM solutions (Table 1) in the ITCZ region. Note that in Figures 7b and 7d, we plotted out the effects of wind stress and wind speed separately to better identify the contribution from each forcing.

[38] On both the MJO and submonthly timescales, SST variability is dominated by wind forcing (stress plus speed). The SST variations caused by the MJO (solid black curve in Figure 7a) and by the submonthly ISOs (solid black curve in Figure 7c) are well reproduced by wind-forced SST (red curves in Figures 7a and 7c), with correlation coefficients

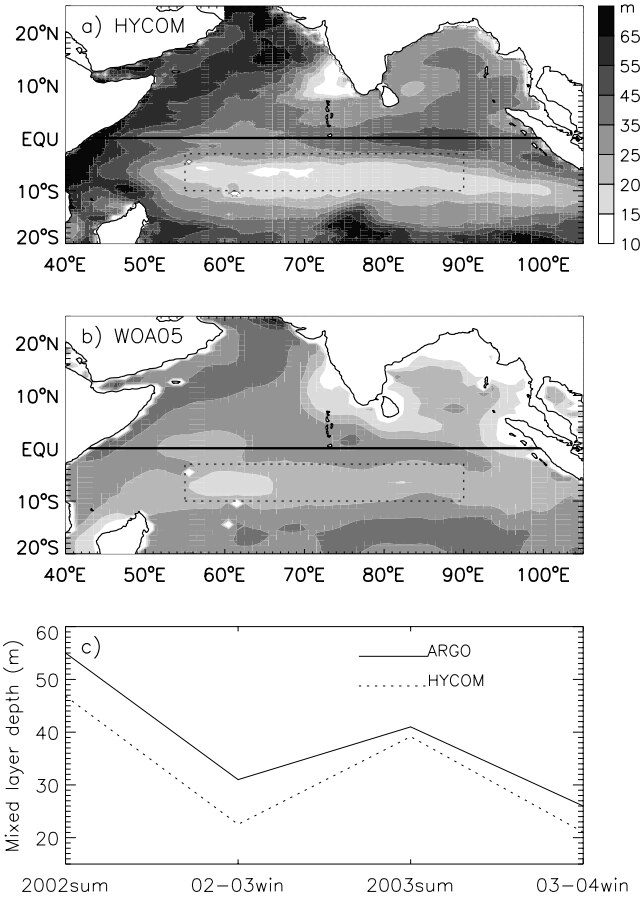

Figure 6. (a) Surface mixed layer depth averaged over the winters of 1999–2003 from HYCOM MR. It is defined as the depth where density increases (relative to surface density) by an amount that is equivalent to a 0.5°C temperature decrease. (b) Same as Figure 6a but for the mixed layer depth derived from the WOA05 climatology. Note that near Sumatra and the Bay of Bengal coasts, WOA05 has very few data points, and thus the estimated mixed layer depths may not be reliable in these regions. (c) Observed (derived from ARGO data)/HYCOM mixed layer depth averaged over the ITCZ region (the boxed area in Figures 6a and 6b) from summer 2000 to winter 2003. The summer season is defined as the mean of May–October, and winter is defined as November–April. Units are m.

between the dark and red curves of $r_{wind} = 0.95$ above 95% significance for both the MJO and submonthly periods. The correlations between the dark and red curves in the warm pool are 0.93 and 0.95 on the MJO and submonthly timescales, respectively, and 0.97 and 0.96 in the western-central equatorial basin (not shown).

[39] The dominant wind forcing results almost equally from wind stress and wind speed (solid and dashed curves in Figures 7b and 7d). The correlation between the SSTs forced by total wind (red curve) and stress only (solid black curve) is 0.87 at the MJO periods and 0.89 at submonthly periods. Similar correlation for wind speed (dashed curve) is 0.88 on both the MJO and submonthly timescales. The SST STD is 0.15°C for wind stress and 0.16°C for wind speed at the MJO periods.

[40] Wind speed attains the maximum amplitude and wind stress curl is strong in the ITCZ region (Figure 1), where the mixed layer is thin (Figure 6) [*McCreary et al.*, 1993; *Murtugudde et al.*, 1999; *Xie et al.*, 2002]. Strong winds act on a thin mixed layer, producing the SST maximum (Figure 3 and Table 2). In the warm pool, wind speed associated with the ISOs also reaches the maximum. The corresponding SST variation, however, is only half of the amplitude of the ITCZ region at the MJO periods (Table 2 and Figure 4). This is likely because the surface mixed layer is much thinner in the ITCZ than the warm pool (Figure 6), which quickens the surface cooling/warming because the same amount of flux acts on a thinner layer. It also enhances entrainment because the cold thermocline water is entrained into the thin surface layer. In the western-central equatorial ocean, wind speeds appear to be weaker than they are in the other two regions. The amplitude of SST change, however, is larger than that of the warm pool. The most likely reason is that the atmosphere is more humid and closer to saturation in the warm pool because of its high SST than in the western-central equatorial basin (not shown). As a result, latent heat flux is larger in the western equatorial ocean for the same wind speed. As shall be discussed later, advection can also have significant contribution in this region.

[41] Interestingly, although submonthly ISOs have larger variances in winds than the MJO (Figure 1), SST changes caused by the MJO generally have larger amplitudes especially over the ITCZ (Figures 3 and 5). This is because it is the time derivative of SST, more so than SST itself, is proportional to the strength of the forcing. If we only consider response of SST to a heat flux change induced by local wind speed and ignore advection terms, amplitudes of the SST are proportional to both the wind strength and

Table 2. STDs of Filtered TRMM and HYCOM SST (Parentheses) Averaged Over Three Representative Regions of the Indian Ocean (Boxes in Figure 3c) During Northern Winter[a]

	10–90 Day, deg C	30–90 Day, deg C	10–30 Day, deg C
Region 1, ITCZ area	0.39 (0.47)	0.34 (0.42)	0.19 (0.20)
Region 2, warm pool	0.25 (0.23)	0.19 (0.19)	0.16 (0.13)
Region 3, west EQ	0.30 (0.32)	0.23 (0.27)	0.18 (0.17)

[a]First, the 3-day TRMM and HYCOM MR SST data for the period of 1998–2004 are band-pass filtered at 10–90 day, 30–90 day, and 10–30 day periods. Then the SST values at each period range are averaged over region 1 in the ITCZ, region 2 in the warm pool, and region 3 in the western-central equatorial basin, respectively. Finally, the STD is calculated for each region at each period band for the winter months of 5 years (November–April of 1999–2003). Data for 1998 and 2004 are excluded to remove the end point effects of the filter.

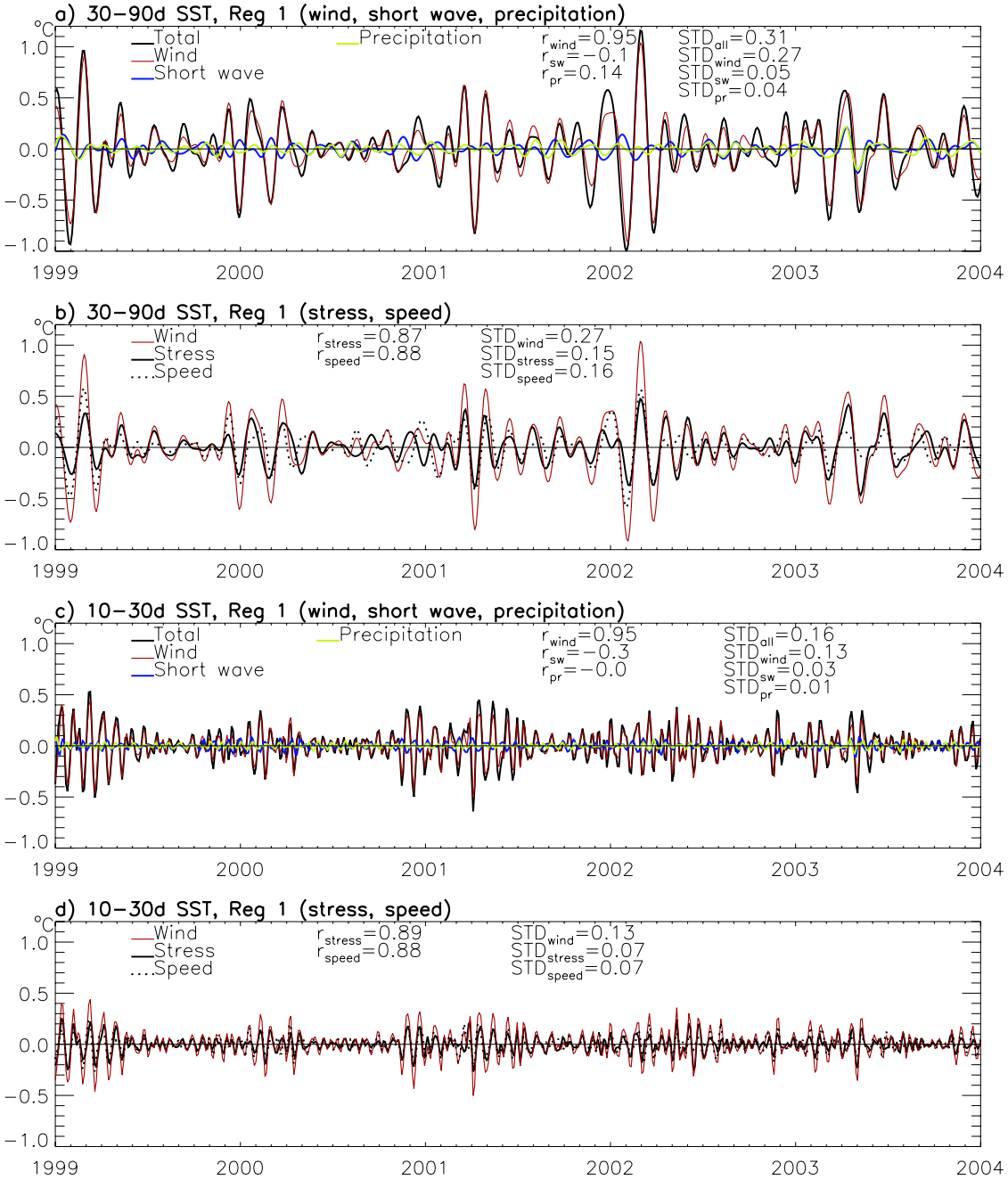

Figure 7. (a) Time series of 30–90 day SST averaged over the ITCZ region (region 1) forced by total ISO (*MR* − *EXP*1, black curve), total wind (*MR* − *EXP*4, red curve), short-wave radiation (*MR* − *EXP*5, blue curve), and precipitation (*MR* − *EXP*6, green curve) for the period of interest. Units are °C. (b) Same as Figure 7a but for SST caused by wind stress (*MR* − *EXP*3, solid black curve) and wind speed (*EXP*3 − *EXP*4, dashed curve). For comparison, SST forced by total wind is repeated (red curve). (c) Same as Figure 7a but for 10–30 day SST. (d) Same as Figure 7b but for 10–30 day SST.

length of forcing period, similar to the current response to local winds demonstrated by *Han* [2005]. For a simple case with a constant heat flux, the longer the period, the larger the SST variation. Physically, this means that for oscillating winds, a longer period allows the ocean to heat or cool for a longer time before the wind switches phase. Even though the 10–30 day winds have larger amplitudes than 30–90 day winds, the latter can cause a larger SST variation because its period is about 3 times of the former.

[42] Variability of solar radiation generally causes much weaker SST changes with an opposite sign (blue curves in Figures 7a and 7c). Simultaneous correlations between the SST variation induced by the total MJO (solid curve) and that caused only by short-wave radiation (blue curve) are $r_{sw} = -0.1$ for both the ITCZ and western-central equatorial

regions. The most significant influence of MJO short-wave flux is in the warm pool, where $r_{sw} = -0.4$. At submonthly periods, the correlations between SSTs induced by total ISO and by solar radiation (black and blue curves in Figure 7c) are $r_{sw} = -0.3$, -0.6, and -0.2 in the ITCZ, warm pool, and western-central equatorial ocean, respectively. The relative amplitude, $STD_{sw}/STD_{all} = 0.2$, is also the largest in the warm pool for both the MJO and submonthly ISOs. The weaker effects of solar radiation may result partly from the weaker intraseasonal variation of the ISCCP flux (section 2.2). This error, however, is expected to be small because the underestimation is only about 14%.

[43] Precipitation associated with the ISOs causes even weaker SST changes, with STD_{pr} being smaller than STD_{sw} (green curves in 7a, c) especially in the warm pool and western-central basin (not shown). This result is consistent with the conclusions of *Shinoda and Hendon* [1998] based on a 1-D model results and *Waliser et al.* [2003, 2004] derived by examining effects of the composite canonical MJO.

3.4.2. Strong MJO Events

[44] To demonstrate the basin-scale SST structure associated with strong MJO events, we analyze many cases on the basis of the strong cooling in the ITCZ region (Figure 4a). Here we discuss the January 1999 cooling event in detail, in order to compare with, and provide process analysis for, existing case studies of *Harrison and Vecchi* [2001] and *Duvel et al.* [2004].

[45] Figure 8 shows 30–90 day wind and OLR (left column), TRMM SST (middle), and HYCOM MR SST during 1 January to 15 February 1999 at a 9 day interval. Strong convection associated with the MJO propagates eastward (left column). On 1 January prior to the convection, the ocean warms up by a significant magnitude near the ITCZ region in both the observations and HYCOM MR. By 10 January, strong convection occurs in the Indian Ocean and propagates eastward (10–28 January plots). Associated with the eastward propagation of convection are strong westerly winds with the maximum amplitude over the ITCZ. These intraseasonal westerlies reinforce the mean seasonal westerlies (Figure 2). After the convection and strong winds, the ocean cools by over 1°C in the ITCZ. By 6 and 15 February, positive OLR anomalies appear over the Indian Ocean. Winds are weak or reverse to become easterlies over the ITCZ region, which act to weaken the seasonal mean westerlies. As a result, SST begins to increase. The observed SST amplitude and structure are well simulated by HYCOM.

[46] Figure 9 plots the 30–90 day SST forced by the MJO during the peak warming phase on 1 January and peak-cooling phase on 28 January (Figures 9a and 9b). Consistent with our discussion above, effects of intraseasonal winds dominate short-wave flux and precipitation, with both wind speed and stress playing important roles (Figures 9c–9l). During the peak-warming phase, wind speed weakens over the ITCZ and western equatorial ocean (dashed curves in Figure 9e). This reduced wind speed coincides with the warm SST in these regions, suggesting that the reduced wind decreases turbulent heat fluxes and entrainment cooling and therefore warms up the ocean. Note that the wind speed contours shown in Figure 9 are 6 days before the SST. This is because it is the time derivative (or change) of SST, rather than the SST itself, is directly proportional to the turbulent heat flux and entrainment cooling. As a result, SST maxima often lag wind maxima. Simultaneous and 3 day lead wind speeds are also analyzed, and they are very similar to those shown in Figure 9, with slight differences in some regions. During the peak-cooling phase, the enhanced wind speed (solid curves in Figure 9f) increases turbulent heat fluxes and entrainment cooling. The importance of entrainment is also evidenced in Figure 10, which shows a shallower (thicker) mixed layer due partly to the weakened (enhanced) entrainment during the warm (cold) phase of the event.

[47] Like the wind speed, intraseasonal wind stress also causes significant SST variability. First, Ekman pumping velocity (line contours in Figures 9g and 9h), defined as $w_c = \frac{\partial}{\partial x}\left(\frac{\tau^y}{f}\right) - \frac{\partial}{\partial y}\left(\frac{\tau^x}{f}\right)$, causes local upwelling (solid curves) or downwelling (dashed curves) and thus increases or decreases SST. In the above, τ^x and τ^y are the zonal and meridional wind stress and f is the Coriolis parameter. For the reason discussed above, the 30–90 day w_e shown in Figure 10 is from 6 days before the SST. In some regions, however, w_e and SST do not agree, and on the equator w_e is undefined, indicating the influence of other processes associated with wind stress forcing. Intraseasonal wind stress drives strong intraseasonal currents, advecting the mean and intraseasonal SST (Figures 11a–11d). For example, in the western-central equatorial basin where mean SST gradients are large, intraseasonal currents carry the warmer water westward during the warm phase and colder water equatorward during the cold phase (Figures 11a and 11b), contributing to the SST variation in this region. Apparently, both intraseasonal and seasonal currents can advect intraseasonal SST and thus can modify the intraseasonal SST variability (Figures 11c–11f).

[48] Intraseasonal wind stress also forces equatorial waves, which can affect the SST remotely. During the MJO warm phase, Rossby waves excited by the MJO wind have low sea level in the central-eastern equatorial basin and high sea level in the western-central ocean (Figure 12, top). The high sea level anomaly (SLA), which indicates a deepened thermocline, in the western-central equatorial basin can reduce upwelling and thus contribute to the warm SST in this region (9g). On 28 January, the low SLA propagates westward to 65°E–70°E, induces upwelling and contributes to the maximum cooling there. The speed of propagation is approximately 55 cm/s, which is very close to the speed of the first meridional mode, second baroclinic mode Rossby wave [*Han*, 2005]. In addition, easterly (westerly) wind components along the equator during the warm (cool) phase of the MJO (left plots of Figure 8) act to shallow (deepen) the mixed layer near the equator (not shown), which may help to enhance the warming phase but weaken the cooling.

[49] Solar radiation has a much weaker influence relative to winds (compare Figures 9i and 9j with Figures 9c and 9d). At specific locations, however, its influence can be significant. Near 90°E and south of the equator, short-wave radiation cools the SST by ~ -0.5°C. The influence of intraseasonal precipitation, which can affect the SST through the barrier layer effect, is small (Figures 9k and 9l).

[50] Note that although convection and winds associated with the MJO propagate eastward (Figure 8, left), apparent

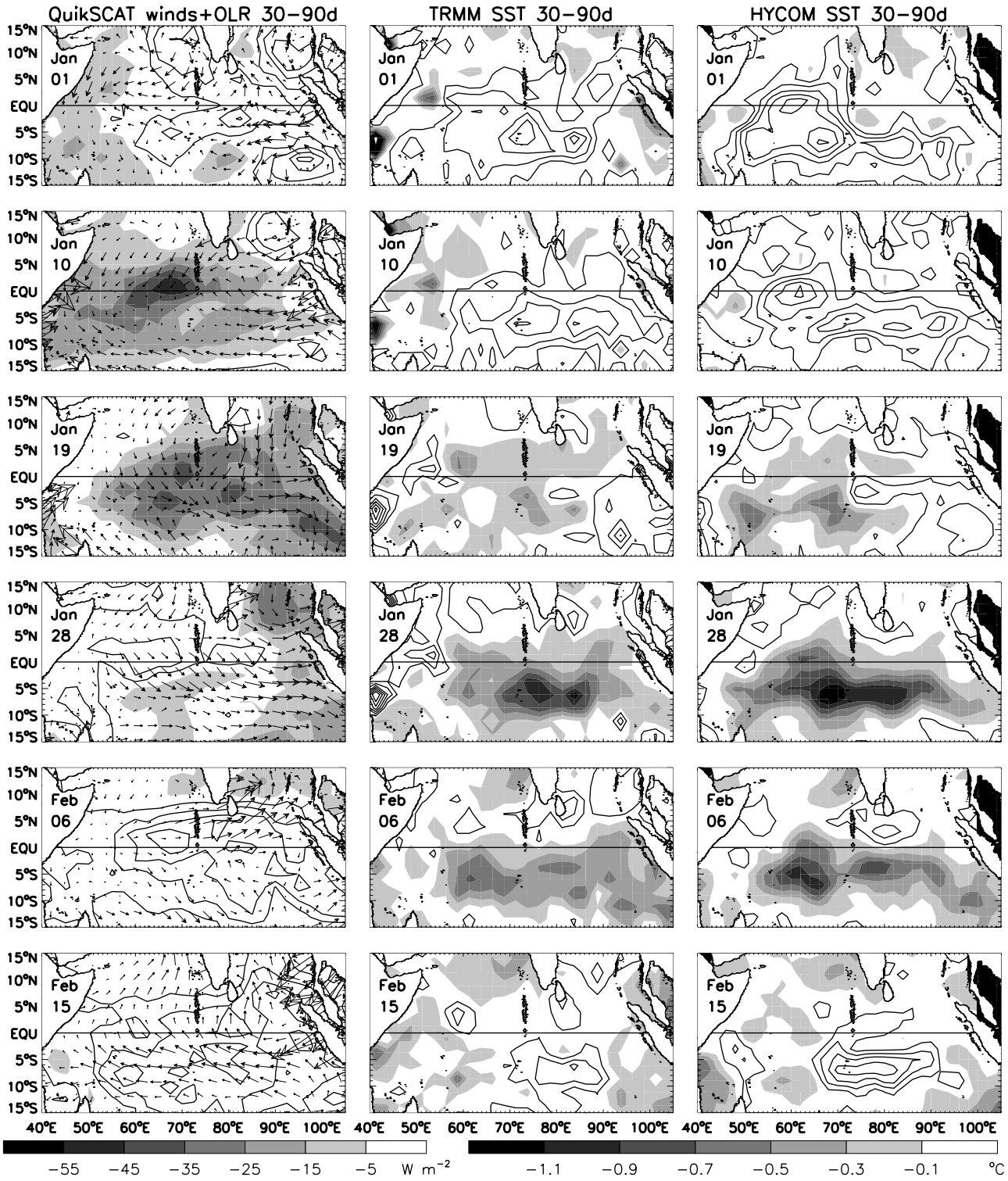

Figure 8. (left) The 30–90 day filtered QuikSCAT wind stress (arrows) and OLR (shading) for a MJO event during 1 January to 15 February 1999 at a 9-day interval. (middle) TRMM 30–90 day SST for the same period of time. (right) HYCOM 30–90 day SST for the same period of time. Positive SST values are contoured and negative ones are shaded, with an interval of 0.2°C. Units are dyn cm^{-2} for wind stress and W m^{-2} for OLR.

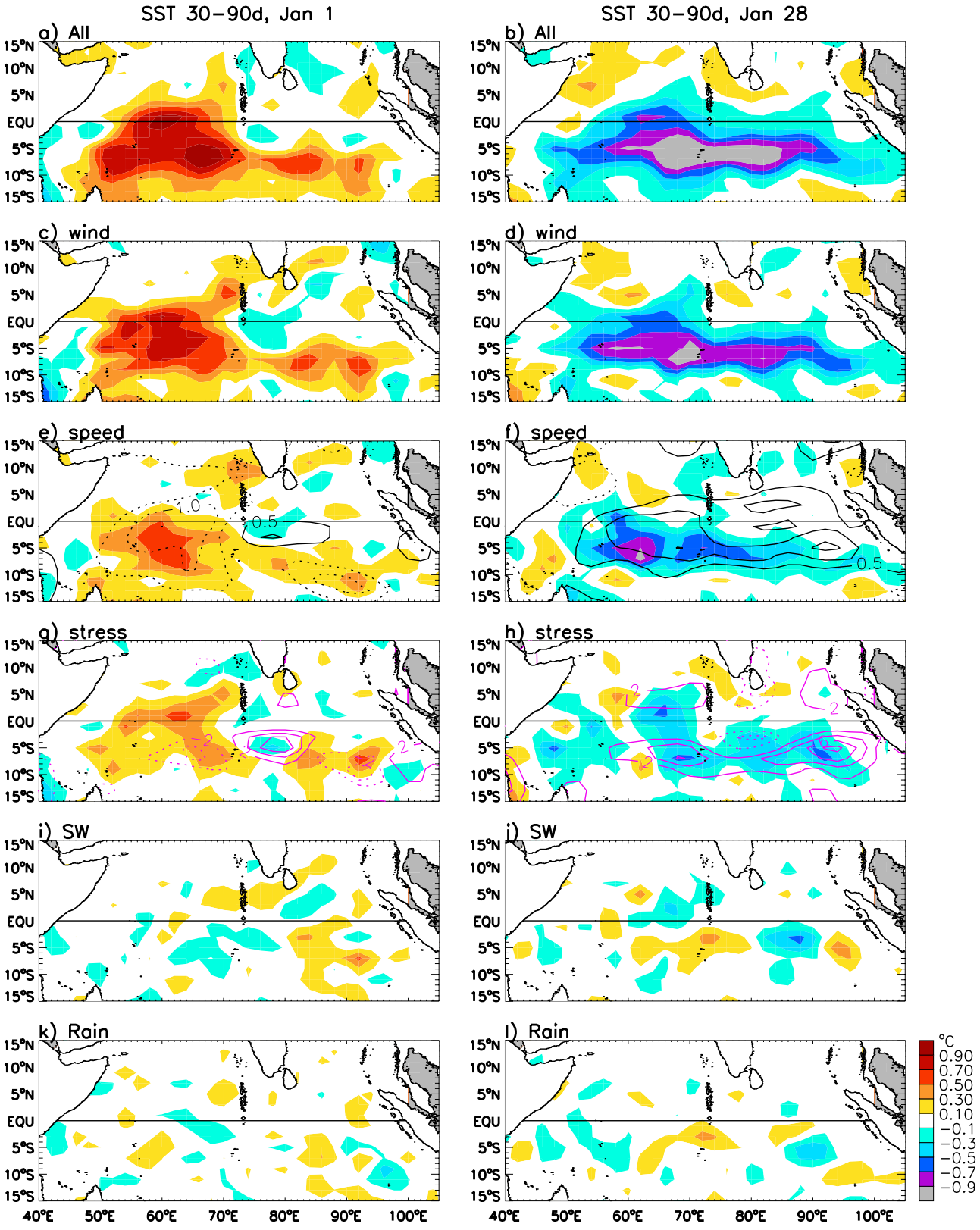
SST 30–90d, Jan 1
SST 30–90d, Jan 28
a) All
b) All
c) wind
d) wind
e) speed
f) speed
g) stress
h) stress
i) SW
j) SW
k) Rain
l) Rain
15°N
10°N
5°N
EQU
5°S
10°S
15°S
40°E
50°E
60°E
70°E
80°E
90°E
100°E
1.0
0.5
0.5
2
2
2
2
°C
0.90
0.70
0.50
0.30
0.10
−0.1
−0.3
−0.5
−0.7
−0.9

Figure 9

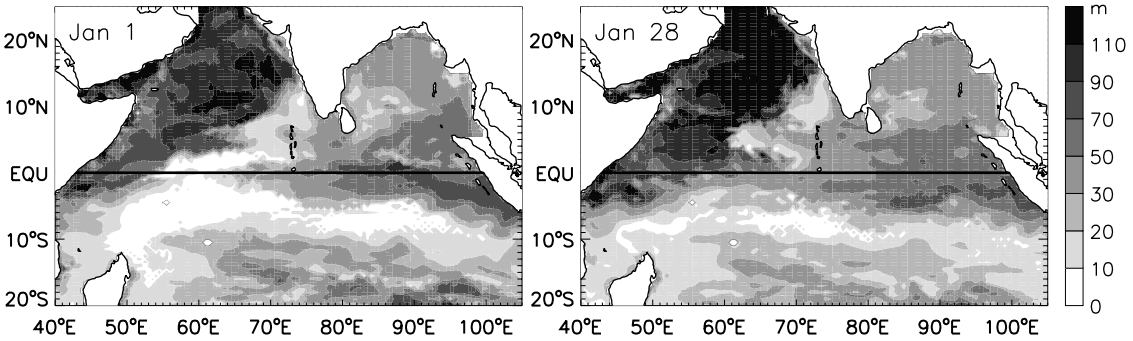

Figure 10. Mixed layer thickness for (left) 1 January and (right) 28 January 1999 from HYCOM MR solution. Units are m.

eastward propagation of SST only occurs in the central-eastern basin near the ITCZ region (Figure 8, 19 January to 6 February of the middle and right plots). This is likely because the MJO winds have a basin scale and thus causes across-basin simultaneous cooling. In addition, oceanic Rossby waves propagate westward in the central and western basin (Figure 12), which act to against eastward propagation of SST in these regions.

3.4.3. Strong Submonthly ISO Events

[51] To demonstrate the difference of SST structures caused by the submonthly ISOs and the MJO, Figure 13 shows the 10–30 day OLR and wind stress (left), TRMM SST (middle), and HYCOM MR SST (right) during 27 January to 11 February 2003 at a 3 day interval. In contrast to the MJO which shows a basin-scale convection, submonthly ISOs exhibit Rossby and Kelvin wave structures: with double maxima of OLR amplitude off the equator in the central basin and a single maximum in the eastern equatorial ocean. The double OLR maxima and associated winds appear to propagate westward and also somewhat southward (compare plots for 27 and 30 January and 2–8 February), which is likely the convectively coupled, first meridional mode Rossby wave modified by the mean flow, as suggested by *Chatterjee and Goswami* [2004]. The single OLR maximum in the eastern equatorial basin appears to propagate southeastward.

[52] Similar to the MJO, submonthly ISOs cause a largest SST change near the ITCZ, where winds are strong (left column) and the mixed layer is thin. Different from the MJO, submonthly ISOs cause a distinct SST structure over the Indian Ocean, and the SST signals propagate along with the ISOs. For example, when the strong easterly winds associated with the ISOs in the ITCZ region propagate southwestward (27 January to 2 February plots), the positive SST anomaly also propagates southwestward. Similarly, the negative SST over the ITCZ propagates southwestward during 5–11 February, as the strong winds associated with the ISO moves southwestward. In the eastern ocean warm pool, SST begins to cool on 30 January in responding to the cyclonic winds associated with the negative OLR. As the cyclone moves southeastward along the coast of Sumatra, SST cooling also appears to move southeastward (compare the 30 January to 5 February plots of TRMM and MR SST). Analysis of the suite of HYCOM experiments demonstrates that effects of winds dominate submonthly SST variability, with both wind speed and wind stress playing important roles (not shown).

4. Summary and Discussion

[53] In this paper, impacts of atmospheric boreal winter ISOs on intraseasonal variability of the Indian Ocean SST are investigated by analyzing satellite data and performing OGCM experiments. The 3 day mean QuikSCAT winds and daily OLR are used to document the MJO and submonthly ISOs (Figures 1, 8, and 13). The 3 day mean TRMM SST data are analyzed to provide observational evidence for SST variability. To understand the processes involved, a suite of OGCM experiments are performed covering the period of 1998–2004 using an Indian Ocean version of HYCOM (Table 1).

[54] The maximum variability of intraseasonal SST occurs in the south equatorial ocean in the wintertime ITCZ region, because the strong forcing by the maximum wind acts on a very thin surface mixed layer (Figures 1, 3, and 6), as suggested by *Duvel et al.* [2004] and *Saji et al.* [2006]. The observed, maximum intraseasonal warming (cooling) associated with strong ISO events can be 1.13°C (−0.97°C) when averaged over (60°E–85°E, 10°S–3°S), and the wintertime STD for the period of interest is 0.39°C (Figure 4 and Table 2). In the warm pool where intraseasonal winds

Figure 9. The 30–90 day filtered SST for (left) 1 January and (right) 28 January 1999 from a suite of HYCOM solutions designed to isolate processes. (a and b) SST forced by the MJO (*MR* − *EXP*1). (c and d) SST forced by the MJO wind (speed plus stress). (e and f) SST forced by the MJO wind speed only. Overlying on the SST are the 30–90 day wind speed (line contours) 6 days before the SST. Dashed lines show negative values, which indicate weak wind speed, and solid lines are positive values, which indicate strong wind speed. (g and h) SST forced by the MJO wind stress. Overlying on the SST are the 30–90 day Ekman pumping velocity, w_e. See text for definition. Positive values are solid and negative ones are dashed. (i and j) SST forced by the MJO short-wave flux. (k and l) SST forced by the MJO precipitation. Units are °C for SST, m s^{-1} for wind speed, and 10^{-6} m s^{-1} for w_e.

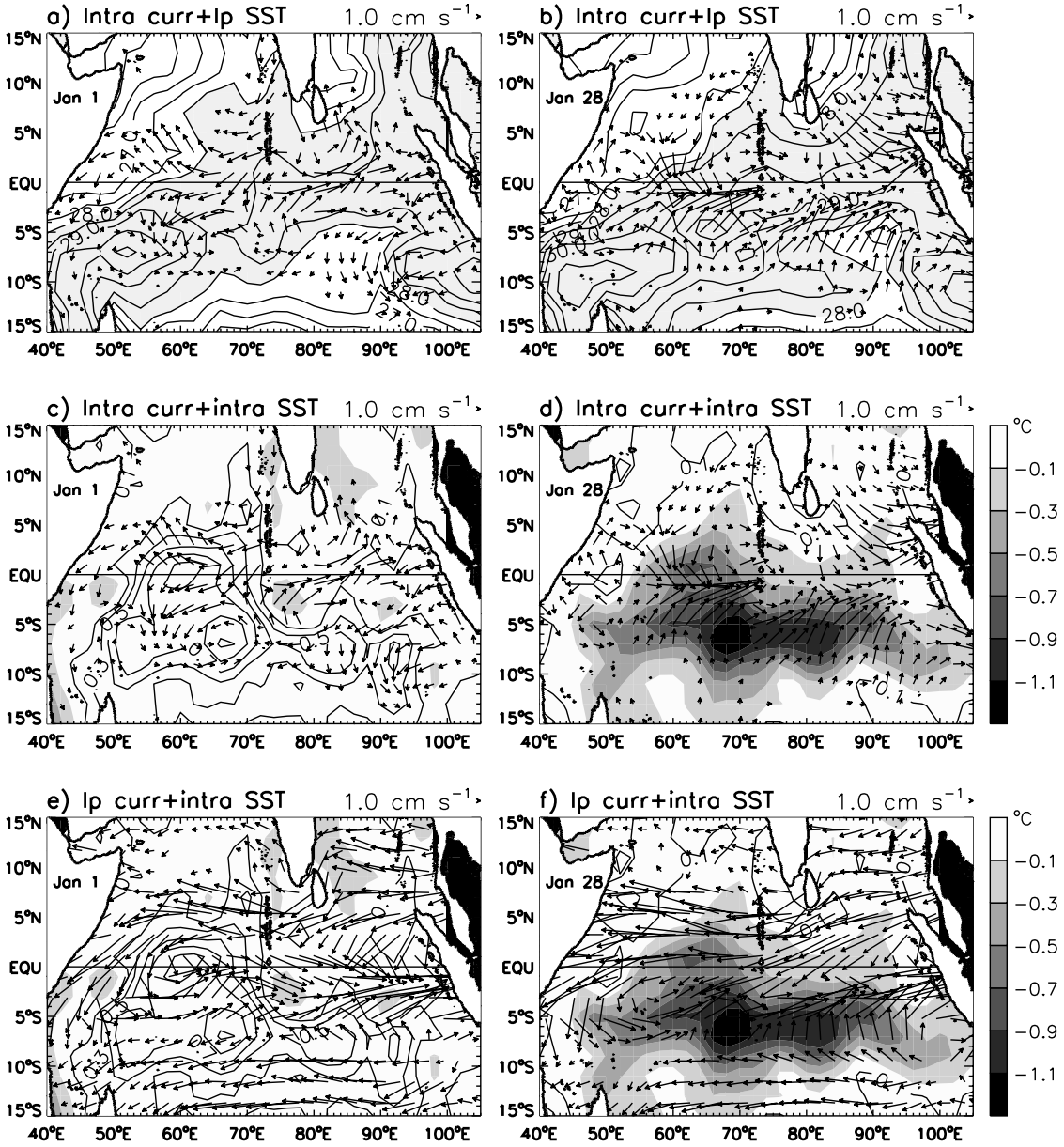

Figure 11. (a) The 30–90 day currents (arrows) forced by the MJO from solution (*MR* − *EXP*1) superimposed on seasonal SST from EXP1 (contours) for 1 January 1999, which shows intraseasonal currents advecting seasonal SST. Values higher than 28°C are shaded. (b) Same as Figure 11a but for 28 January. (c) Same as Figure 11a but for replacing the seasonal SST by 30–90 day SST from HYCOM MR, demonstrating intraseasonal currents advecting intraseasonal SST on 1 January. Positive SST values are contoured and negative ones are shaded, with an interval of 0.2°C. (d) Same as Figure 11c but for 28 January. (e) Same as Figure 11c but for replacing the intraseasonal currents by seasonal currents from EXP1, showing seasonal currents advecting intraseasonal SST. Currents smaller than 5 cm s^{-1} are suppressed. (f) Same as Figure 11e but for 28 January.

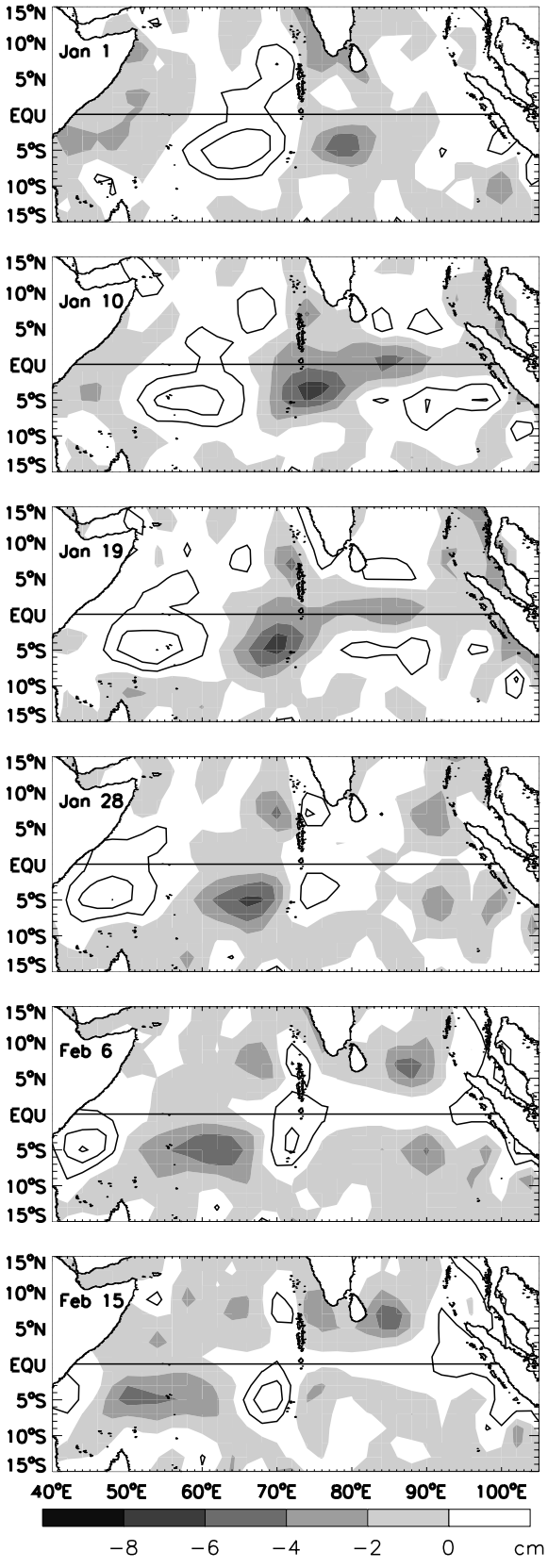

Figure 12. The 30–90 day sea level anomaly (SLA) from solution *MR − EXP*1, showing Rossby waves forced by the MJO during 1 January to 15 February at a 9-day interval. Positive values are contoured and negative ones are shaded, with an interval of 2 cm.

are equally strong, intraseasonal SST is much weaker. This is because the mixed layer is much thicker in the warm pool area, which slows down the surface warming and cooling processes. In the western-central equatorial basin where intraseasonal winds are weak, the SST variations are stronger than those of the warm pool. This is likely because the unsaturated atmosphere in the western equatorial basin enhances evaporation and the strong mean SST gradients in this region give rise to strong advection.

[55] The maximum variability of intraseasonal SST over the ITCZ region results largely from the MJO forcing (Figures 4a and 5). This is interesting because the submonthly ISOs have somewhat stronger winds than the MJO (Figure 1 and region 1 in Figure 3c). The likely reason is that the response of SST to a local, periodic forcing is proportional to both the forcing strength and length of the forcing period [*Han*, 2005]. Even though the MJO winds are somewhat weaker, the SST can be larger because of the longer periods of the MJO. In the western-central equatorial basin and especially in the eastern Indian Ocean warm pool where submonthly winds are much stronger (regions 3 and 2 in 3c), however, SST variations at submonthly periods have comparable amplitudes to those at the MJO periods (Figures 3e, 3g, and 5 and Table 2).

[56] On both the MJO and submonthly timescales, winds are the dominant forcing for SST variability (Figures 7 and 9), with both surface heat fluxes and oceanic processes playing important roles. Intraseasonal wind speed causes changes in latent and sensible heat fluxes at the surface and entrainment of colder water from the subsurface, affecting the SST (Figures 9 and 10). Intraseasonal wind stress affects the SST through various oceanic processes. Locally, positive (negative) Ekman pumping velocity associated with wind stress curl causes upwelling (downwelling) in off-equatorial regions, such as the south equatorial basin in the ITCZ region (Figures 9g and 9h), increasing the surface cooling (warming). Intraseasonal wind stress can also drive strong intraseasonal currents, causing SST variations through advection (Figure 11). This effect is large in the western equatorial ocean where both the SST gradients and intraseasonal currents are strong. Remotely, Rossby waves forced by the wind stress associated with the ISOs propagate westward (Figure 12), causing variability of the thermocline and thus affecting the upwelling. Additionally, intraseasonal wind stress can change mixed layer depth and thus affect intraseasonal SST.

[57] Short-wave radiation generally plays a minor role in producing intraseasonal SST variability (Figures 7, 9i, and 9j), with the maximum $STD_{sw}/STD_{all} = 0.2$ occurring in the warm pool region for both the MJO and submonthly ISOs. At specific locations for some events, its effects can be significant. The effects of intraseasonal precipitation appear to be negligible, consistent with the result of *Shinoda and Hendon* [1998] and *Waliser et al.* [2003].

[58] While strong MJO events cause basin-wide warming/cooling with maxima occurring in the ITCZ region (Figure 8), strong submonthly ISOs generate SST variability with a more complex structure and propagate with the ISOs (Figure 13). Submonthly SST variability propagates southwestward with the convectively coupled Rossby waves and southeastward with Kelvin waves. The dominance of winds over solar radiation and precipitation, the importance of

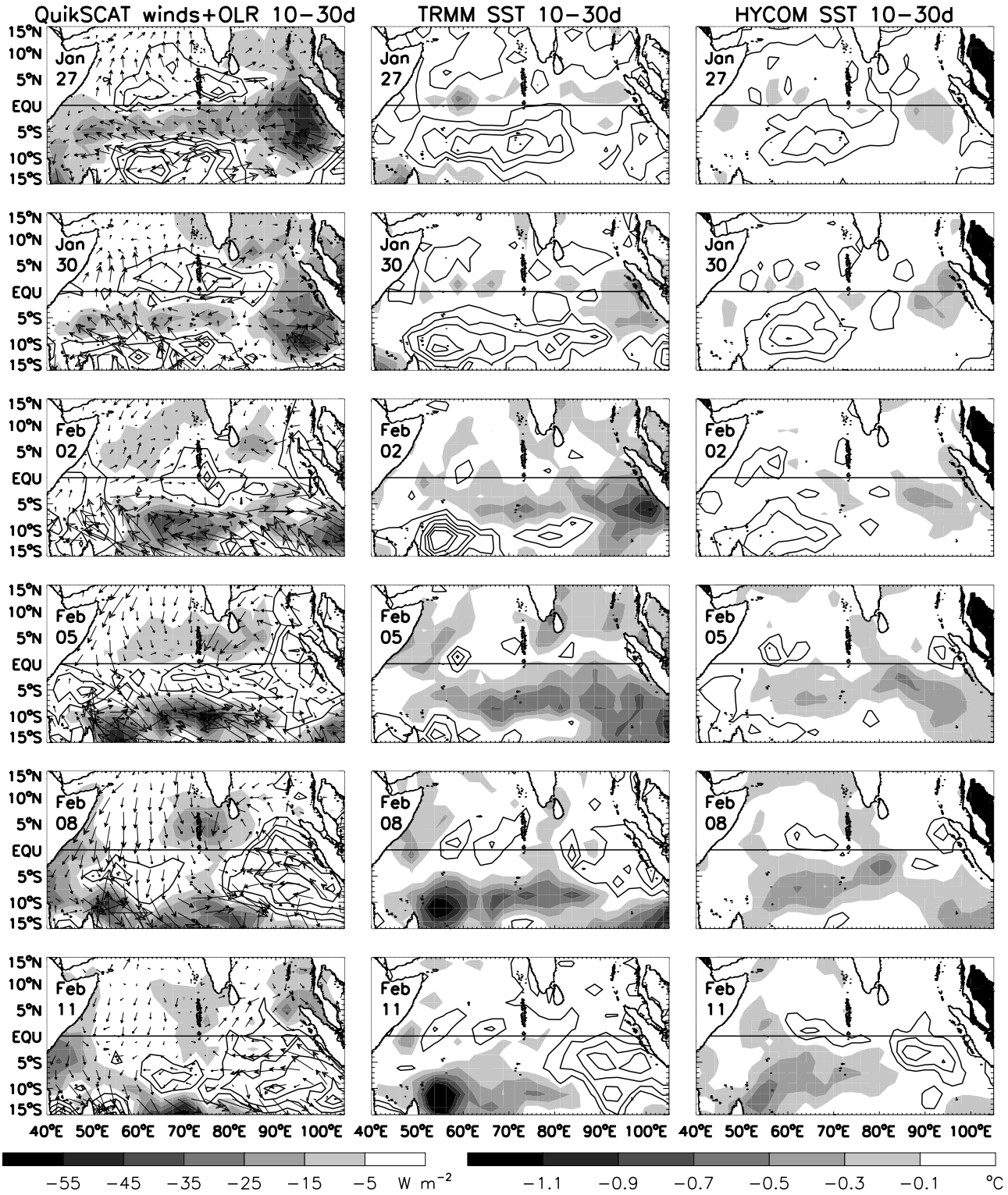

Figure 13. Same as Figure 8 but for submonthly ISOs during 27 January to 11 February 2003 with a 3-day interval.

wind-induced surface heat fluxes and oceanic processes, and the different SST patterns at the MJO and submonthly periods may have important implications on air-sea interaction processes for the MJO and submonthly ISOs over the tropical Indian Ocean.

[59] **Acknowledgments.** We thank ECMWF and NCAR for the ERA-40 fields, NOAA-CIRES Climate Diagnostics Center for the CMAP precipitation, and Yuanchong Zhang for the ISCCP flux data. Appreciation also goes to Toshiaki Shinoda for the helpful discussions, Wendy Tang for preparing the QuikSCAT wind fields, and Hui Zhu for preparing the ARGO data. The ARGO data were collected and made freely available by the International Argo Project and the national programs that contribute to it.

We also thank NODC for making the WOA05 data available through the Internet. Weiqing Han is supported by NSF OCE-0452917 and NASA Ocean Vector Winds Program award 1283568, Dongliang Yuan is supported by the "100-Expert Program"' of the Chinese Academy of Sciences, W. Timothy Liu is supported by NASA Ocean Vector Winds and Physical Oceanography Programs, and Daria J. Halkides is supported by NSF OCE-0136836 and NSF OCE-0452917.

References

Bhat, G. S., et al. (2001), BOBMEX: The Bay of Bengal Monsoon Experiment, *Bull. Am. Meteorol. Soc.*, *82*, 2217–2243.

Bleck, R. (2002), An oceanic general circulation model framed in hybrid isopycnic-Cartesian coordinates, *Ocean Modell.*, *4*, 55–88.

Chatterjee, P., and B. N. Goswami (2004), Structure, genesis and scale selection of the tropical quasi-biweekly mode, *Q. J. R. Meteorol. Soc.*, *130*, 1171–1194.

Chen, T.-C., and J.-M. Chen (1993), The 10–20 day mode of the 1979 Indian monsoon: Its relation with time variation of monsoon rainfall, *Mon. Weather Rev.*, *121*, 2465–2482.

Duchon, C. E. (1979), Lanczos filtering in one and two dimensions, *J. Appl. Meteorol.*, *18*, 1016–1022.

Duvel, J. P., R. Roca, and J. Vialard (2004), Ocean mixed layer temperature variations induced by intraseasonal convective perturbations over the Indian Ocean, *J. Atmos. Sci.*, *61*, 1004–1023.

Flatau, M., P. J. Flatau, P. Phoebus, and P. P. Niller (1997), The feedback between equatorial convection and local radiative and evaporative processes: The implications for intraseasonal oscillations, *J. Atmos. Sci.*, *54*, 2373–2386.

Fu, X., B. Wang, T. Li, and J. P. McCreary (2003), Coupling between northward propagating, intraseasonal oscillations and sea-surface temperature in the Indian Ocean, *J. Atmos. Sci.*, *60*, 1733–1783.

Gadgil, S., P. N. Vinayachandran, P. A. Francis, and S. Gadgil (2004), Extremes of the Indian summer monsoon rainfall, ENSO and equatorial Indian Ocean oscillation, *Geophys. Res. Lett.*, *31*, L12213, doi:10.1029/2004GL019733.

Halliwell, G. R. (1998), Simulation of North Atlantic decadal/multi-decadal winter SST anomalies driven by basin-scale atmospheric circulation anomalies, *J. Phys. Oceanogr.*, *28*, 5–21.

Halliwell, G. R. (2004), Evaluation of vertical coordinate and vertical mixing algorithms in the Hybrid Coordinate Ocean Model (HYCOM), *Ocean Modell.*, *7*, 285–322.

Han, W. (2005), Origins and dynamics of the 90-day and 30–60 day variations in the equatorial Indian Ocean, *J. Phys. Oceanogr.*, *35*, 708–728.

Han, W., D. M. Lawrence, and P. J. Webster (2001), Dynamical response of equatorial Indian Ocean to intraseasonal winds: Zonal flow, *Geophys. Res. Lett.*, *28*, 4215–4218.

Han, W., P. J. Webster, R. Lukas, P. Hacker, and A. Hu (2004), Impact of atmospheric intraseasonal variability in the Indian Ocean: Low-frequency rectification in equatorial surface current and transport, *J. Phys. Oceanogr.*, *34*, 1350–1372.

Han, W., T. Shinoda, L. Fu, and J. P. McCreary (2006a), Impact of atmospheric intraseasonal oscillations on the Indian Ocean dipole during the 1990s, *J. Phys. Oceanogr.*, *36*, 670–690.

Han, W., W. T. Liu, and J. Lin (2006b), Impact of atmospheric submonthly oscillations on sea surface temperature of the tropical Indian Ocean, *Geophys. Res. Lett.*, *33*, L03609, doi:10.1029/2005GL025082.

Harrison, D. E., and G. A. Vecchi (2001), January 1999 Indian Ocean cooling event, *Geophys. Res. Lett.*, *28*, 3717–3720.

Hendon, H. H., and J. Glick (1997), Intraseasonal air-sea interaction in the tropical Indian and Pacific oceans, *J. Clim.*, *10*, 647–661.

Hendon, H. H., and M. L. Salby (1994), Planetary-scale circulations forced by intraseasonal variations of observed convection, *J. Atmos. Sci.*, *53*, 1751–1758.

Hendon, H. H., B. Liebmann, and J. D. Glick (1998), Oceanic Kelvin waves and the Madden-Julian Oscillation, *J. Atmos. Sci.*, *55*, 88–101.

Inness, P. M., and J. M. Slingo (2003), Simulation of the Madden-Julian Oscillation in a coupled general circulation model. part I: Comparison with observations and an atmosphere-only GCM, *J. Clim.*, *16*, 345–364.

Jerlov, N. G. (1976), *Marine Optics*, 231 pp., Elsevier, New York.

Jochum, M., and R. Murtugudde (2005), Internal variability of Indian Ocean SST, *J. Clim.*, *18*, 3726–3738.

Jones, C., D. E. Waliser, and C. Gautier (1998), The influence of the Madden-Julian Oscillation on ocean surface heat fluxes and sea surface temperature, *J. Clim.*, *11*, 1057–1072.

Kemball-Cook, S., and B. Wang (2001), Equatorial waves and air-sea interaction in the boreal summer intraseasonal oscillation, *J. Clim.*, *14*, 2923–2942.

Kessler, W. S. (2005), The oceans, in *Intraseasonal Variability in the Atmosphere-Ocean Climate System*, edited by W. K. M. Lau and D. E. Waliser, pp. 175–222, Springer, New York.

Kessler, W. S., and R. Kleeman (2000), Rectification of the Madden-Julian Oscillation into the ENSO cycle, *J. Clim.*, *13*, 3560–3575.

Kiladis, G., and K. Straub (2001), Forcing of the equatorial ocean by an atmospheric Kelvin wave, in *Proceedings of the 13th Conference on Atmospheric and Oceanic Fluid Dynamics*, pp. 283–286, Am. Meteorol. Soc., Breckenridge, Colo.

Kiladis, G. N., and K. M. Weickmann (1997), Horizontal structure and seasonality of large-scale circulations associated with submonthly tropical convection, *Mon. Weather Rev.*, *125*, 1997–2013.

Kindle, J. C., and J. D. Thompson (1989), The 26- and 50-day oscillations in the western Indian Ocean: Model results, *J. Geophys. Res.*, *94*, 4721–4736.

Knutson, T. R., and K. M. Weickmann (1987), 30–60 day atmospheric oscillations: Composite life cycles of convection and circulation anomalies, *Mon. Weather Rev.*, *115*, 1407–1436.

Krishnamurti, T. N., and D. Subramanyam (1982), The 30–50 day mode at 850 mb during MONEX, *J. Atmos. Sci.*, *39*, 2088–2095.

Krishnamurti, T. N., D. K. Oosterhof, and A. V. Mehta (1988), Air-sea interaction on the time scale of 30 to 50 days, *J. Atmos. Sci.*, *45*, 1304–1322.

Large, W. G., J. C. McWilliams, and S. C. Doney (1994), Oceanic vertical mixing: A review and a model with a nonlocal boundary layer parameterization, *Rev. Geophys.*, *32*, 363–403.

Large, W. G., G. Danabasoglu, S. C. Doney, and J. C. McWilliams (1997), Sensitivity to surface forcing and boundary layer mixing in a global ocean model: Annual-mean climatology, *J. Phys. Oceanogr.*, *27*, 2418–2447.

Lau, K. M., and P. H. Chan (1985), Aspects of the 40–50 day oscillation during the northern winter as inferred from outgoing long wave radiation, *Mon. Weather Rev.*, *113*, 1889–1909.

Lau, K. M., and D. E. Waliser (Eds.) (2005), *Intraseasonal Variability in the Atmosphere-Ocean Climate System*, Springer, New York.

Lawrence, D. M., and P. J. Webster (2002), The boreal summer intraseasonal oscillation: Relationship between northward and eastward movement of convection, *J. Atmos. Sci.*, *59*, 1593–1606.

Levitus, S., and T. P. Boyer (1994), *World Ocean Atlas 1994*, vol. 4, *Temperature, NOAA Atlas NESDIS 4*, 129 pp., NOAA, Silver Spring, Md.

Levitus, S., R. Burgett, and T. P. Boyer (1994), *World Ocean Atlas 1994*, vol. 3, *Salinity, NOAA Atlas NESDIS 3*, 111 pp., NOAA, Silver Spring, Md.

Li, T., and B. Wang (1994), The influence of sea surface temperature on tropical intraseasonal oscillation: A numerical study, *Mon. Weather Rev.*, *122*, 2349–2362.

Lin, J. L., et al. (2006), Tropical intraseasonal variability in 14 IPCC AR4 climate models. part I: Convective signals, *J. Clim.*, *19*, 2665–2690.

Madden, R. A., and P. R. Julian (1971), Detection of a 40–50 day oscillation in the zonal wind of the tropical Pacific, *J. Atmos. Sci.*, *28*, 702–708.

Madden, R. A., and P. R. Julian (1972), Description of global-scale circulation cells in the tropics with a 40–50 day period, *J. Atmos. Sci.*, *29*, 1109–1123.

Masumoto, Y., H. Hase, Y. Kuroda, H. Matsuura, and K. Takeuchi (2005), Intraseasonal variability in the upper layer currents observed in the eastern equatorial Indian Ocean, *Geophys. Res. Lett.*, *32*, L02607, doi:10.1029/2004GL021896.

Matthews, A. J. (2000), Propagation mechanisms for the Madden-Julian Oscillation, *Q. J. R. Meteorol. Soc.*, *126*, 2637–2652.

McBride, J. (1987), The Australian summer monsoon, in *Reviews of Monsoon Meteorology*, edited by C. P. Chang and T. N. Krishnamurti, pp. 203–231, Oxford Univ. Press, New York.

McCreary, J. P., P. K. Kundu, and R. L. Molinari (1993), A numerical investigation of dynamics, thermodynamics, and mixed-layer processes in the Indian Ocean, *Prog. Oceanogr.*, *31*, 181–224.

McPhaden, M. J. (1982), Variability in the central equatorial Indian Ocean. part 1: Ocean dynamics, *J. Mar. Res.*, *40*, 157–176.

McPhaden, M. J. (1999), Genesis and evolution of the 1997–98 El Niño, *Science*, *283*, 950–954.

Miyama, T., J. P. McCreary, D. Sengupta, and R. Senan (2006), Dynamics of biweekly oscillations in the equatorial Indian Ocean, *J. Phys. Oceanogr.*, *36*, 827–846.

Moore, A. M., and R. Kleeman (1999), Stochastic forcing of ENSO by the intraseasonal oscillation, *J. Clim.*, *12*, 1199–1220.

Murakami, T., and M. Frydrych (1974), On the preferred period of upper wind fluctuations during the summer monsoon, *J. Atmos. Sci.*, *31*, 1549–1555.

Murtugudde, R., S. Signorini, J. Christian, A. Busalacchi, and C. McClain (1999), Ocean color variability of the tropical Indo-Pacific basin

observed by SeaWiFS during 1997–1998, *J. Geophys. Res.*, *104*, 18,351–18,366.
Murtugudde, R., J. P. McCreary, and A. J. Busalacchi (2000), Oceanic processes associated with anomalous events in the Indian Ocean with relevance to 1997–1998, *J. Geophys. Res.*, *105*, 3295–3306.
Numaguti, A. (1995), Characteristics of 4- to 20-day period disturbances observed in the equatorial Pacific during the TOGA COARE IOP, *J. Meteorol. Soc. Jpn.*, *73*, 353–377.
Rao, S. A., and T. Yamagata (2004), Abrupt termination of Indian Ocean dipole events in response to intraseasonal disturbances, *Geophys. Res. Lett.*, *31*, L19306, doi:10.1029/2004GL020842.
Reppin, J., F. A. Schott, J. Fischer, and D. Quadfasel (1999), Equatorial currents and transports in the upper central Indian Ocean: Annual cycle and interannual variability, *J. Geophys. Res.*, *104*, 15,495–15,514.
Saji, N. H., B. N. Goswami, P. N. Vinayachandran, and T. Yamagata (1999), A dipole mode in the tropical Indian Ocean, *Nature*, *401*, 360–363.
Saji, N. H., S.-P. Xie, and C.-Y. Tam (2006), Satellite observations of intense intraseasonal cooling events in the tropical south Indian Ocean, *Geophys. Res. Lett.*, *33*, L14704, doi:10.1029/2006GL026525.
Schiller, A., and J. S. Godfrey (2003), Indian Ocean intraseasonal variability in an ocean general circulation model, *J. Clim.*, *16*, 21–39.
Schouten, M. W., W. P. M. de Ruijter, P. J. van Leeuwen, and H. A. Dijkstra (2002), An oceanic teleconnection between the equatorial and southern Indian Ocean, *Geophys. Res. Lett.*, *29*(16), 1812, doi:10.1029/2001GL014542.
Sengupta, D., B. N. Goswami, and R. Senan (2001a), Coherent intraseasonal oscillations of ocean and atmosphere during the Asian summer monsoon, *Geophys. Res. Lett.*, *28*, 4127–4130.
Sengupta, D., R. Senan, and B. N. Goswami (2001b), Origin of intraseasonal variability of circulation in the tropical central Indian Ocean, *Geophys. Res. Lett.*, *28*, 1267–1270.
Shinoda, T., and W. Han (2005), Influence of the Indian Ocean dipole on atmospheric subseasonal variability, *J. Clim.*, *18*, 3891–3909.
Shinoda, T., and H. H. Hendon (1998), Mixed layer modeling of intraseasonal variability in the tropical western Pacific and Indian oceans, *J. Clim.*, *11*, 2668–2685.
Shinoda, T., H. H. Hendon, and J. Glick (1998), Intraseasonal variability of surface fluxes and sea surface temperature in the tropical western Pacific and Indian oceans, *J. Clim.*, *11*, 1685–1702.
Sikka, D. R., and S. Gadgil (1980), On the maximum cloud zone and the ITCZ over Indian longitudes during southwest monsoon, *Mon. Weather Rev.*, *108*, 1840–1853.
Slingo, J. M., et al. (1996), Intraseasonal oscillations in 15 atmospheric general circulation models: Results from an AMIP diagnostic subproject, *Clim. Dyn.*, *12*, 325–357.
Sperber, K. R., S. Gualdi, S. Legutke, and V. Gayler (2005), The Madden-Julian Oscillation in ECHAM4 coupled and uncoupled general circulation models, *Clim. Dyn.*, *25*, 117–140.
Sprintal, J., and M. Tomczak (1992), Evidence of the barrier layer in the surface layer of the tropics, *J. Geophys. Res.*, *97*, 7305–7316.
Takayabu, Y. N., T. Iguchi, M. Kachi, A. Shibata, and H. Kanzawa (1999), Abrupt termination of the 1997–98 El Niño in response to a Madden-Julian Oscillation, *Nature*, *402*, 279–282.
Tang, W., and W. T. Liu (1996), Objective interpolation of scatterometer winds, *Publ. 96-19*, 16 pp., Jet Propul. Lab., Pasadena, Calif.
Tsai, P. T. H., J. J. O'Brien, and M. E. Luther (1992), The 26-day oscillation observed in the satellite sea surface temperature measurements in the equatorial western Indian Ocean, *J. Geophys. Res.*, *97*, 9605–9618.
Vincent, D. G., A. Fink, J. M. Schrage, and P. Speth (1998), High- and low-frequency intraseasonal variance of OLR on annual and ENSO timescales, *J. Clim.*, *11*, 968–986.
Waliser, D. E., K. M. Lau, and J.-H. Kim (1999), The influence of coupled sea surface temperatures on the Madden-Julian Oscillation: A model perturbation experiment, *J. Atmos. Sci.*, *56*, 333–357.
Waliser, D. E., R. Murtugudde, and L. E. Lucas (2003), Indo-Pacific Ocean response to atmospheric intraseasonal variability: 1. Austral summer and the Madden-Julian Oscillation, *J. Geophys. Res.*, *108*(C5), 3160, doi:10.1029/2002JC001620.
Waliser, D. E., R. Murtugudde, and L. E. Lucas (2004), Indo-Pacific Ocean response to atmospheric intraseasonal variability: 2. Boreal summer and the Intraseasonal Oscillation, *J. Geophys. Res.*, *109*, C03030, doi:10.1029/2003JC002002.
Wang, B., and H. Rui (1990), Synoptic climatology of transient tropical intraseasonal convection anomalies: 1975–1985, *Meteorol. Atmos. Phys.*, *44*, 43–61.
Wang, B., and X. Xie (1997), A model for the boreal summer intraseasonal oscillation, *J. Atmos. Sci.*, *54*, 72–86.
Wang, B., and X. Xie (1998), Coupled modes of the warm pool climate system. part I: The role of air-sea interaction in maintaining Madden-Julian Oscillation, *J. Clim.*, *11*, 2116–2135.
Webster, P. J. (1983), Mechanisms of monsoon transition: Surface hydrology effects, *J. Atmos. Sci.*, *40*, 2110–2124.
Webster, P. J., and C. Hoyos (2004), Prediction of monsoon rainfall and river discharge on 15-30 day time scales, *Bull. Am. Meteorol. Soc.*, *85*, 1745–1765.
Webster, P. J., A. M. Moore, J. P. Loschnigg, and R. R. Leben (1999), Coupled ocean-atmosphere dynamics in the Indian Ocean during 1997–1998, *Nature*, *401*, 356–360.
Webster, P. J., et al. (2002), The JASMINE pilot study, *Bull. Am. Meteorol. Soc.*, *83*, 1603–1630.
Wentz, F. J., C. Gentemann, D. Smith, and D. Chelton (2000), Satellite measurements of sea surface temperature through clouds, *Science*, *288*, 847–850.
Wheeler, M., and G. N. Kiladis (1999), Convectively coupled equatorial waves: Analysis of clouds and temperature in the wavenumber-frequency domain, *J. Atmos. Sci.*, *56*, 374–399.
Wheeler, M. C., and J. L. McBride (2005), Australian-Indonesian monsoon, in *Intraseasonal Variability in the Atmosphere-Ocean Climate System*, edited by W. K. M. Lau, and D. E. Waliser, pp. 125–173, Springer, New York.
Woolnough, S. J., J. M. Slingo, and B. J. Hoskins (2000), The relationship between convection and sea surfaced temperature on intraseasonal timescales, *J. Clim.*, *13*, 2086–2104.
Woolnough, S. J., J. M. Slingo, and B. J. Hoskins (2001), The organization of tropical convection by intraseasonal sea surface temperature anomalies, *Q. J. R. Meteorol. Soc.*, *127*, 887–907.
Xie, P., and P. A. Arkin (1996), Analyses of global monthly precipitation using gauge observations, satellite estimates, and numerical model predictions, *J. Clim.*, *9*, 840–858.
Xie, S.-P., H. Annamalai, F. Schott, and J. P. McCreary (2002), Structure and mechanisms of south Indian Ocean climate variability, *J. Clim.*, *15*, 864–878.
Yasunari, T. (1981), Structure of an Indian summer monsoon system with around 40-day period, *J. Meteorol. Soc. Jpn.*, *59*, 336–354.
Zhang, Y., W. B. Rossow, A. A. Lacis, V. Oinas, and M. I. Mishchenko (2004), Calculation of radiative fluxes from the surface to top of atmosphere based on ISCCP and other global data sets: Refinements of the radiative transfer model and the input data, *J. Geophys. Res.*, *109*, D19105, doi:10.1029/2003JD004457.

D. J. Halkides, Department of Atmospheric and Oceanic Sciences, University of Colorado, 51 Murray St., Mt. Morris, NY 14510, USA.
W. Han, Department of Atmospheric and Oceanic Sciences, University of Colorado, Campus Box 311, Boulder, CO 80309, USA. (whan@enso.colorado.edu)
W. T. Liu, JPL, California Institute of Technology, 4800 Oak Grove Dr., Pasadena, CA 91109, USA.
D. Yuan, Institute of Oceanology, Chinese Academy of Sciences, 7 Nanhai Road, Qingdao 266071, China.